Mechanical Engineering Advances 2025, 3(2), 2486.
https://doi.org/10.59400/mea2486

Article

The SG6043 airfoil optimization for low Reynolds number applications in wind turbines

Hossein Seifi Davari[1], Mohammad Yaghoub Abdollahzadeh Jamalabadi[1,*], Mohsen Seify Davari[2]

[1] Ocean Engineering Department, Chabahar Maritime University, Chabahar 99717, Iran
[2] Germi Department, Islamic Azad University, Germi 56911, Iran
*** Corresponding author:** Mohammad Yaghoub Abdollahzadeh Jamalabadi, my.abdollahzadeh@cmu.ac.ir, muhammad_yaghoob@yahoo.com

CITATION

Davari HS, Jamalabadi MYA, Davari MS. The SG6043 airfoil optimization for low Reynolds number applications in wind turbines. Mechanical Engineering Advances. 2025; 3(2): 2486. https://doi.org/10.59400/mea2486

ARTICLE INFO

Received: 31 December 2024
Accepted: 7 March 2025
Available online: 8 April 2025

Abstract: This study focuses on optimizing the SG6043 airfoil for small wind turbines (SWTs) operating at low Reynolds numbers (Re = 100,000 to 600,000). Using XFOIL software, 71 airfoils were analyzed, and the SG6043 airfoil demonstrated the highest lift-to-drag ratio (C_L/C_D). Three modified airfoils were designed by varying the thickness-to-camber ratio (t/c) between 0.5 and 1.5. The SG6043 modified 1 airfoil achieved a maximum C_L/C_D of 184.85 at Re = 600,000, outperforming other airfoils. These findings provide valuable insights for designing more efficient SWTs for low wind speed applications. At first, 71 airfoils, including some symmetrical National Advisory Committee for Aeronautics (NACA) 4-digit, NACA 5-digit, Eppler series, Selig series, and other airfoils with higher aerodynamic performance at Reynolds numbers (Re) of 100,000 to 600,000 (the operation range for small wind turbines, SWTs), were chosen and analyzed in XFOIL software to determine their lift-to-drag ratio (C_L/C_D). The results showed that the SG6043 airfoil had the highest maximum C_L/C_D when compared to the other airfoils. To investigate and enhance the shape modification of the airfoil utilizing variations in thickness-to-camber ratio (t/c) and to determine the ideal t/c at Re of 100,000 to 600,000, the SG6043 airfoil was used. Based on the findings, 0.5 to 1.5 was the optimum t/c at Re of 100,000 to 600,000 for the development of the SG6043 airfoil, which had the maximum C_L/C_D. Then, three airfoils with varying thicknesses and cambers were designed and analyzed at the mentioned Re, with the optimal t/c being between 0.5 and 1.5. The findings indicated that when the Re increased, the SG6043 modified airfoil's aerodynamic efficiency enhanced. SG6043 modified 1 airfoil presented the greatest C_L/C_D of 184.85 at a Re of 600,000. For the SG6043 modified 2 airfoil, the maximum stall angle (AoA_{stall}) of 13° was demonstrated for Re of 300,000 to 600,000. Maximum C_L/C_D values for SG6043 modified 1, SG6043 modified 3, and SG6043 modified 2 were 184.85, 182.36, and 177.25, respectively. SG6043 modified 2, SG6043 modified 1, and SG6043 modified 3 had peak lift coefficients (C_L) of 1.798, 1.79, and 1.788, respectively. SG6043 modified airfoils performed well in the drag bucket when initial lift increases were accompanied by either steady or decreasing drag.

Keywords: modified airfoil; Reynolds numbers; aerodynamic; lift-to-drag; optimization; XFOIL software

1. Introduction

Small wind turbines (SWTs) are increasingly used for decentralized power generation, particularly in remote areas with low wind speeds. However, SWTs operate at low Reynolds numbers (Re), which poses challenges for aerodynamic efficiency. Most airfoil designs are optimized for large wind turbines operating at higher Re, making them unsuitable for SWTs. This study aims to optimize the SG6043 airfoil for low Re applications by varying the thickness-to-camber ratio (t/c) to improve aerodynamic performance. The results provide a foundation for designing

more efficient SWTs for low wind speed conditions. A device that transforms wind power into electrical energy is a wind turbine (WT). Depending on the demands and purposes, WTs can be put in oceans and on beaches to generate power for residential homes [1]. SWTs operate at low Re due to their small size and position. Airfoils are crucial to the efficacy of WTs, and for greater efficiency, airfoils must be employed. It has also been demonstrated that SWTs function at Re below 500,000 and that lower wind speeds also function within this range. WT efficiency will decrease if low-aerodynamic-efficiency airfoils are employed [2]. As well as, study results have demonstrated that airfoils made for giant wind turbines are inappropriate for SWTs. WTs must operate well to have high aerodynamic efficiency since it depends on the C_L, drag coefficient (C_D), C_L/C_D, drag bucket, and AoA_{stall} [3]. A number of studies have been investigated recently to improve the effectiveness of VAWTs using a variety of airfoils and methods, as follows:

Seifi et al. [4] used the XFOIL software to conduct studies on several NACA and Selig airfoil types at low Re. Their results demonstrated that the NACA0015 airfoil surpassed other airfoils regarding maximum C_L/C_D. The NACA0015 airfoil's shape, camber, and thickness were then modified, and a novel airfoil was developed and compared to the original airfoil. Their research showed that for the NACA0015 modified airfoil at Re of 35780 and 53670, the maximum C_L/C_D increased by 34.01% and 17.94%, respectively. Giguere et al. [5] proved that thinner airfoils were more efficient than thicker airfoils, and as the Re increased, the C_L/C_D of airfoils increased.

Using the Class Deformation Method (CST) and the Parametric Cross Section Parameterization Method (PARSEC), Akram et al. [6] were able to raise the C_L and C_L/C_D by 11.8% and 9.6%, respectively. Martel et al. [7] used a multi-objective Non-Dominated Sorting Genetic Algorithm (SGA) to optimize the airfoil of a UAV in their research. Then, the optimization algorithm was combined with an updated CST parameterization to enhance aerodynamic efficiency by increasing C_L/C_D. Their results showed an enhancement in aerodynamic efficiency of up to 65.3% in C_L/C_D at an AoA of 8° compared to the base airfoil.

Wu et al. [8] studied the standard aerodynamic shape optimization with the proposed POD-based CST airfoil-dependent process, and their findings showed that the developed parametric method was able to closely correspond to the initially high-dimensional CST method's capacity to include the potential airfoils with significantly fewer parameters, which was capable of resolving the conflict between the high-dimensional design parameters and an increase in optimization challenges.

The optimum airfoil for VAWTs at low tip speed ratios (TSR), when dynamic stall existed, was investigated by Tirandaz et al. [9]. To determine the overall design space, their study used an integrated evaluation of three shape-defining parameters, notably the airfoil's greatest thickness and its location, in addition to the leading-edge radius. Their findings demonstrated an entirely related effect between the three shape-defining parameters on the WT power and thrust coefficients.

The Initial Dolphin Airfoil, the Smooth Transition Dolphin Airfoil, and the Deflected Dolphin Airfoil were three different novel airfoils that were developed by Huang et al. [10] after studying the motion behavior of dolphins. After that, CFD simulations were used to compare the aerodynamic efficiency of these three novel airfoils with the NACA0018 profile. Their findings demonstrated that, in comparison

to the NACA0018 profile, the aerodynamic capabilities of all three kinds of dolphin-head-shaped airfoils were considerably dissimilar due to variations in the curvature and leading edge radius. Osei et al. [11] were able to enhance the maximum C_L/C_D of the EYO7-8, EYO8-8, and EYO9-8 airfoils by 134, 131, and 127, respectively, by introducing three airfoils by altering the shape of the SG6043 airfoil with XFOIL software. Additionally, they revealed in the follow-up research that the aerodynamic efficiency of the airfoils under study improved as the Re rose [12].

Hu et al. [13] utilized the free-form deformation method to modify the airfoil shape using control points and sensitivity analysis to condense the size of the control variables. Since altering the geometry of the airfoil was able to offer both stability and the highest C_L/C_D, it was similar to doing single-objective optimization while under a constraint. Their findings demonstrated that static stability height and C_L/C_D were sensitive to abrupt changes around the leading edge, one-quarter chord point, and trailing edge. The deformed ideal airfoil with an S-shape camber line decreased the C_L/C_D to achieve sufficient static stability.

Santos et al. [14] investigated the advantages of the Bézier-GAN as an airfoil parameterization approach for H-Darrieus turbines in an effort to eliminate these shortcomings. They employed sensitivity evaluation, metamodeling, and optimization techniques in addition to computational fluid dynamics (CFD) models. Their findings demonstrated that the Bézier-GAN integrated well with the framework under investigation and significantly reduced the study's overall cost of computation. Shape optimization is a significant phase in aerodynamics, yet it is computationally costly to use CFD simulation programs in the optimization procedure by Achour et al. [15].

As well as, to enhance convergence, Lim et al. [16] investigated multi-objective aerodynamic optimization problems using a hybrid evolutionary-adaptive directional localization method. Their findings revealed that the adaptive directional search process significantly improves convergence for issues where the directional search was effective and minimizes computational spending for cases where the directional search did not produce competitive findings.

Findings by Guo et al. [17] showed that an improved shuttle-shaped airfoil was able to further efficiently reduce the aerodynamic C_D and at the same time enhance the prototype blade's performance in tests when compared to elliptical airfoils. The aim of Boudis et al.'s [18] optimization process was to enhance the WT output power, and the aim was to pick the S809 airfoil C_L/C_D with three Re of 3×10^5, 4.8×10^5, and 10^6 at *AoAs* between 0° to 20°. Their finding showed that (i) the C_L/C_D of the optimized airfoils was noticeably enhanced compared to the original S809 airfoil; (ii) this enhancement was sensitive to the Re; and (iii) the C_L/C_D was moreover enhanced for *AoA* values.

Particle swarm optimization was used by Echavarria et al. [19] along with XFOIL software and the free and open-source CFD OpenFOAM to optimize the airfoil form as parameterized by the NACA 4-digit equations. Then an analysis and comparison of the XFOIL software and CFD simulation followed. In addition to having an effect on the best feasible aerodynamic effectiveness, their findings indicated a linear link between the desired C_L and the highest possible camber of the ideal airfoil. Rangriz et al. [20] used the enhanced geometric parameter method, which was a state-of-the-art airfoil design methodology, along with the non-dominated SGA for the optimization

of airfoils for WT utilization. Then, Pareto-optimal fronts and corresponding optimal airfoil profiles at various peak thickness ratios were acquired. Their results showed that the optimized airfoils were designed in a shape reminiscent of flapped airfoils, which indicated a multi-element airfoil design.

Turbine blade optimization is crucial for several reasons, as it directly impacts the performance, efficiency, durability, and cost-effectiveness of turbines used in various industries, such as aerospace, power generation, and marine propulsion. Here are the key reasons why turbine blade optimization is important:

1) Improved efficiency

Turbine blades are critical components in converting fluid or gas energy into mechanical energy. Optimizing their shape, material, and design enhances aerodynamic efficiency, reducing energy losses and improving overall turbine performance.

Better efficiency translates to higher power output for the same input energy, which is particularly important in power plants and aircraft engines.

2) Reduced fuel consumption

In gas turbines (e.g., jet engines or power plants), optimized blades reduce fuel consumption by improving combustion efficiency and minimizing energy losses.

Lower fuel consumption reduces operational costs and environmental impact, making turbines more sustainable.

3) Enhanced durability and reliability

Turbine blades operate under extreme conditions, including high temperatures, pressures, and mechanical stresses. Optimization ensures they can withstand these conditions without failure.

Improved durability reduces the risk of blade fatigue, cracking, or erosion, leading to longer operational lifespans and fewer maintenance requirements.

4) Cost savings

Optimized blades reduce manufacturing and maintenance costs by minimizing material waste and extending the lifespan of components.

Efficient turbines also lower operational costs by reducing fuel consumption and downtime.

5) Environmental impact

Optimized turbine blades contribute to lower emissions by improving combustion efficiency and reducing fuel consumption.

This is particularly important in industries like aviation and power generation, where reducing carbon footprints is a priority.

6) Higher performance in extreme conditions

Turbine blades in jet engines or power plants must perform reliably at high temperatures and rotational speeds. Optimization ensures they maintain performance under these conditions.

Advanced cooling techniques and materials can be incorporated into optimized designs to handle extreme thermal stresses.

7) Weight reduction

In aerospace applications, reducing the weight of turbine blades without compromising strength or performance is critical. Lighter blades improve fuel efficiency and aircraft performance.

Optimization techniques, such as topology optimization, help achieve the ideal balance between weight and strength.

8) Noise reduction

Optimized blade designs can reduce noise generated by turbines, which is particularly important in aviation and wind turbines located near residential areas.

Improved aerodynamics and blade shapes minimize turbulence and noise emissions.

9) Adaptability to advanced technologies

Optimization allows for the integration of advanced materials (e.g., composites, single-crystal alloys) and manufacturing techniques (e.g., additive manufacturing) to create blades with superior performance characteristics.

It also enables the use of computational fluid dynamics (CFD) and finite element analysis (FEA) to simulate and refine designs before physical prototyping.

10) Competitive advantage

Companies that invest in turbine blade optimization gain a competitive edge by offering more efficient, reliable, and cost-effective products.

In industries like aerospace and energy, even small improvements in turbine performance can lead to significant market advantages.

In conclusion, turbine blade optimization is essential for maximizing efficiency, reducing costs, improving durability, and minimizing environmental impact. It enables turbines to operate more effectively under demanding conditions, making it a critical focus area for engineers and researchers in the field of turbomachinery.

As already mentioned, SWTs work at low Re, and several investigations have been carried out in this Re. However, the appropriate *t*/*c* of airfoils in the Re range of 100,000 to 600,000, where airfoils have higher aerodynamic efficiency, has not been researched and ignored. Hence, it was chosen to investigate present research. The objective of the current study is to use the airfoil's *t*/*c* to improve the aerodynamic performance of the airfoil at Re between 100,000 and 600,000. At first, 71 symmetrical NACA 4-digit, NACA 4-digit, NACA 5-digit, Eppler series, Selig series, and other airfoils with greater aerodynamic performance at Re of 100,000 to 600,000 were studied for the current purpose using the XFOIL software. The next step was to develop three new airfoils with the ideal *t*/*c*. Finally, the modified airfoils in the Re above were evaluated in comparison to the SG6043 airfoil and the newly developed airfoils of the EYO-Series airfoils.

In the present study, the aerodynamic efficiency characteristics of the SG6043 modified (SG6043 modified 1, SG6043 modified 2, and SG6043 modified 3) airfoils were investigated at a scope of Re between 10^5 to 6×10^5, in order to identify their improved aerodynamic productivity features within the range of Re and to determine their aerodynamic efficiency features across the spectrum. The results of this study serve as a starting point for the creation of other low Re airfoils and illustrate important aerodynamic features of the SG6043 modified airfoils. The following section describes the procedures used to carry out this study.

2. Methodology

2.1. Selection and investigation of airfoils

Seventy-one airfoils, including NACA 4-digit, NACA 5-digit, Eppler, and Selig series, were selected for analysis. These airfoils were chosen based on their performance at low Re, which is typical for SWTs. The SG6043 airfoil was identified as the most efficient and was selected for further optimization. A gradient-based form optimization approach is developed in the current study to enhance WT blades. The 2D potential airflow solver with viscous effects, XFOIL software, was utilized with the blade element momentum (BEM) approach. The goal function of the gradient-based optimization procedure was the power output of the WT, which was calculated by the BEM analysis. A number of researchers utilized XFOIL software to develop and design airfoils, and it was demonstrated that it was in good agreement with the experimental results [21–25].

Firstly, 71 commonly used airfoils that have been tested in recent studies were chosen and analyzed in XFOIL software to determine their C_L/C_D at Re of 100,000 to 600,000. A summary of the airfoil selection procedure is shown in **Figure 1**, followed by an analysis using the XFOIL software. The selected airfoils were from symmetrical NACA 4-digit (NACA0010, NACA0012, NACA0015, NACA0018, NACA0020, NACA0021, NACA0022, NACA0025, and NACA0030), NACA 4-digit (NACA2415, NACA2421, NACA3530, NACA4412, NACA4415, NACA4418, NACA5513, NACA6712, and NACA8412), NACA 5-digit (NACA23012, NACA23015, NACA23018, NACA23024, NACA24012, NACA24015, NACA24020, NACA63018, and NACA63415), Selig airfoils (S809, S814, S818, S821, S822, S823, S825, S828, S85, S1046, S1223, S2027, S4083, S5010, S6063, S7012, S8036, S8052, SA7035, SA7038, SD2030, SD6060, SD7003, SD7032, SD7037, SD7062, SD7080, SG6040, SG6041, SG6042, SG6043, SG6050, and SG6051), Eppler airfoils (E231, E374, E387, E423, and ESA40), and BW-3, FX63-137, FX74-Cl5-140, PSU94-097, RG15, and USNPS4.

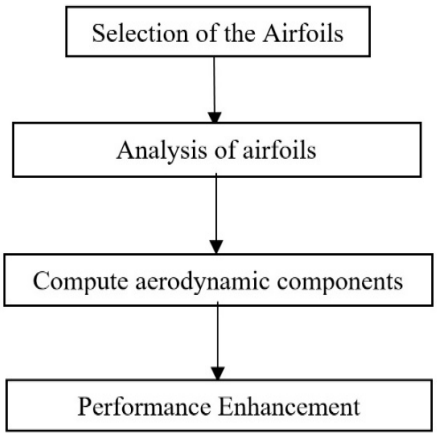

Figure 1. Abstract of XFOIL software for airfoils selection.

2.2. Comparison of the C_L/C_D of airfoils at Rey of 100,000 to 600,000

The aerodynamic performance of the selected airfoils was analyzed using XFOIL software, which is widely used for low Re airfoil analysis due to its accuracy and efficiency. The lift-to-drag ratio (C_L/C_D) was calculated for each airfoil at Re ranging from 100,000 to 600,000. **Figure 2** compares the maximum C_L/C_D for some different airfoils at Re between 100,000 and 600,000. The symmetrical NACA 4-digit airfoils

are presented in **Figure 2a**. The greatest maximum C_L/C_D for the NACA0015 airfoil at Re of 100,000 was 37.32, whereas the lowest maximum C_L/C_D for the NACA0030 airfoil was 12.89. For the airfoils NACA0018, NACA0012, NACA0020, NACA0021, NACA0010, NACA0022, and NACA0025, the maximum C_L/C_D were, respectively, 37.30, 36.6, 36.58, 36.21, 35.71, 35.69, and 32.86. At a Re of 200,000, the NACA0018 and NACA0030 airfoils achieved the highest and lowest maximum C_L/C_D, respectively, at 50.17 and 29.53. NACA0015, NACA0020, NACA0021, NACA0012, NACA0022, NACA0010, and NACA0025 airfoils all had maximum C_L/C_D, respectively, of 49.62, 48.51, 47.63, 47.3, 46.15, 44.81, and 40.09. The highest and lowest maximum C_L/C_D were measured at Re of 300,000, NACA0018, and NACA0030, respectively, and they were 57.21 and 32.05. The corresponding airfoils for the NACA0015, NACA0020, NACA0012, NACA0021, NACA0022, NACA0010, and NACA0025 were 56.83, 54.9, 53.56, 52.43, 50.8, 49.77, and 43.

The highest and lowest maximum C_L/C_D for NACA0015 and NACA0030 airfoils were 62.56 and 35.02, respectively, at a Re of 400,000. The maximum C_L/C_D for the airfoils NACA0018, NACA0020, NACA0012, NACA0021, NACA0022, NACA0010, and NACA0025 were 61.87, 58.9, 57.82, 56.28, 54.67, 53.14, and 45.66, respectively. The highest and lowest C_L/C_D for the NACA0015 and NACA0030 airfoils were 66.44 and 37.21 at a Re of 500,000, respectively. The NACA0018, NACA0020, NACA0021, NACA0012, NACA0022, NACA0010, and NACA0025 airfoils' greatest and lowest maximum C_L/C_D were measured at 66.44, 65.83, 61.89, 61.31, 58.31, 56.39, and 50.16, respectively.

Finally, at the Re of 600,000, the highest and lowest maximum C_L/C_D for the NACA0015 and NACA0030 airfoils were 69.60 and 40.35, respectively. The NACA0018, NACA0020, NACA0012, NACA0021, NACA0022, NACA0010, and NACA0025 airfoils' greatest and lowest maximum C_L/C_D were determined at 68.60, 66.70, 65, 63.70, 61.12, 59.8, and 53.3, respectively. Hence, for the NACA0015 airfoil, the greatest maximum C_L/C_D was recorded at Re of 100,000, 400,000, 500,000, and 600,000, and for the NACA0018 airfoil, the greatest maximum C_L/C_D was recorded at Re of 200,000 and 300,000. Also, the NACA0030 airfoil achieved the lowest maximum C_L/C_D in the range Re of 100,000 to 600,000.

The 4-digit NACA airfoils are depicted in **Figure 2b**. The greatest maximum C_L/C_D for the NACA5513 airfoil at Re of 100,000 was 55.21, while the lowest maximum C_L/C_D for the NACA3530 airfoil was 3.11. NACA4412, NACA6712, NACA4412, NACA2415, NACA8412, NACA2421, and NACA4418 airfoils, in that order, with maximum C_L/C_D of 55.45, 52.81, 46.73, 46.55, 41.52, 36.93, and 35.77. At a Re of 200,000, the NACA5513 and NACA3530 airfoils recorded the highest and lowest maximum C_L/C_D, with values of 85.85 and 36.50, respectively. The maximum C_L/C_D of the airfoils NACA6712, NACA8412, NACA4412, NACA4415, NACA4418, NACA2415, and NACA2421 were, respectively, 79.08, 78.53, 78, 71.9, 64.91, 64.82, and 57.48.

The highest and lowest maximum C_L/C_D were measured at Re of 300,000, NACA5513, and NACA3530, respectively, and they were 103.21 and 41.64. The maximum C_L/C_D airfoils for the NACA8412, NACA4412, NACA4415, NACA6712, NACA4418, NACA2415, and NACA2421 were 95.8, 91.33, 85.74, 82.75, 78.37, 74.9, and 67.13. The greatest and lowest maximum C_L/C_D for NACA5513 and NACA3530

airfoils were 115.69 and 43.28, respectively, at a Re of 400,000. The maximum C_L/C_D for the NACA8412, NACA4412, NACA6712, NACA4415, NACA4418, NACA2415, and NACA2421 airfoils were 106.71, 101.3, 98.53, 96.56, 86.78, 82.54, and 72.35, respectively. The greatest and lowest maximum C_L/C_D for the NACA5513 and NACA3530 airfoils at Re of 500,000 were 124.59 and 44.92, respectively. The NACA8412, NACA4412, NACA4415, NACA6712, NACA4418, NACA2415, NACA2421, and NACA0025 airfoils' maximum C_L/C_D were measured at 116.07, 109.23, 103.63, 102.78, 94.74, 88.89, and 77.37, respectively.

In addition, at the Re of 600,000, the greatest and lowest maximum C_L/C_D for the NACA5513 and NACA3530 airfoils were 131.57 and 46.8, respectively. The NACA6712, NACA8412, NACA4412, NACA4415, NACA4418, NACA2415, and NACA2421 airfoils had a maximum C_L/C_D of 128.93, 122.71, 115.78, 109.56, 100.24, 93.34, and 82.43, respectively. Thus, the NACA5513 airfoil's greatest maximum C_L/C_D was recorded at Re of 100,000 to 600,000, whereas the NACA350030 airfoil had the lowest maximum C_L/C_D at Re of 100,000 to 600,000.

The NACA 5-digit airfoils are displayed in **Figure 2c**. The greatest maximum C_L/C_D for the NACA24012 airfoil at Re of 100,000 was 37.4, whereas the lowest maximum C_L/C_D for the NACA23024 airfoil was 32.06. NACA63415, NACA63018, NACA24015, NACA23012, NACA23015, NACA23018, and NACA24020 airfoils had a maximum C_L/C_D of 36.4, 36.32, 36.3, 35.85, 35.42, and 33.8. The highest and lowest maximum C_L/C_D were achieved by the NACA24012 and NACA23024 airfoils at 56.9 and 43.13, respectively, at a Re of 200,000.

NACA24015, NACA24020, NACA23012, NACA23015, NACA23018, NACA63018, and NACA63415 airfoils' maximum C_L/C_D were 53.5, 50.55, 50.09, 49.18, 48.57, 45.41, and 45.22, respectively. The highest and lowest maximum C_L/C_D were measured at Re of 300,000, NACA24012, and NACA23024, respectively, at 68.87 and 46. The maximum C_L/C_D of the airfoils for the NACA24015, NACA23012, NACA24020, NACA23015, NACA23018, NACA63415, and NACA63018 were 64.77, 61.35, 59.55, 58.39, 56.54, 49.94, and 49.85. The greatest and lowest maximum C_L/C_D for NACA24012 and NACA23024 airfoils were 77.27 and 48.13, respectively, at a Re of 400,000. The maximum C_L/C_D for the NACA24015, NACA23012, NACA23015, NACA24020, NACA23018, NACA63415, and NACA63018 airfoils were 73.19, 69.89, 66.08, 65.96, 63.17, 52.55, and 52.38, respectively.

The highest and lowest maximum C_L/C_D for the NACA24012 and NACA23024 airfoils were 84.06 and 49.95, respectively, at a Re of 500,000. The NACA24015, NACA23012, NACA23015, NACA24020, NACA23018, NACA63018, and NAC63415 airfoils' maximum C_L/C_D were measured at 80.31, 77.7, 72.47, 71.33, 68.86, and 58.14, respectively. Finally, at a Re of 600,000, the greatest and lowest maximum C_L/C_D for the NACA24012 and NACA23024 airfoils were 89.49 and 52.68, respectively. The NACA24015, NACA23012, NACA23015, NACA24020, NACA23018, NACA63415, and NACA63018 airfoils' maximum C_L/C_D were measured at 86.25, 83.4, 78.64, 74.95, 73.7, 63.38, and 63.29, respectively. Hence, the NACA24012 airfoil's greatest maximum C_L/C_D was recorded at Re of 100,000 to 600,000, whereas the NACA23024 airfoil's lowest maximum C_L/C_D was reported at Re of 100,000 to 600,000.

Several of the Selig airfoils are shown in **Figure 2d**. The S825 airfoil had the greatest maximum C_L/C_D of 48.84 at a Re of 100,000, while the S818 airfoil had the lowest maximum C_L/C_D of 14.73. For the airfoils S822, S823, S835, S821, S814, S828, and S809, the maximum C_L/C_D were 41.02, 40.73, 34.17, 33.85, 30.97, 29, and 22.12. At a Re of 200,000, the S825 and S809 airfoils achieved the highest and lowest maximum C_L/C_D, respectively, at 70.12 and 44.41. S822, S823, S814, S835, S818, S821, and S828 airfoils had a maximum C_L/C_D of 67.89, 62.38, 56.3, 54.35, 52.47, 52.3, and 46.87, respectively.

The highest and lowest maximum C_L/C_D were measured at Re of 300,000, S825, and S828, respectively, and they were 81.7 and 48.36. The maximum values for the S822, S823, S814, S818, S835, S821, and S809 airfoils were 75.12, 73.8, 68.45, 67.69, 66.03, 63.07, and 55.35. The maximum C_L/C_D for the S825 and S828 airfoils was 91.98 and 58.09, respectively, at a Re of 400,000. The maximum C_L/C_D for the airfoils S822, S823, S814, S818, S835, S821, and S809 were 86.69, 82.11, 79.32, 75.72, 73.52, 69.82, and 68.01, respectively.

The maximum C_L/C_D for the S825 and S809 airfoils was 96.79 and 73.09, respectively, at the Re of 500,000. The S822, S823, S818, S814, S835, S821, and S828 airfoils' greatest and lowest maximum C_L/C_D were measured at 94.06, 87.96, 85.23, 84.97, 79.06, 75.09, and 74.87, respectively.

Finally, at a Re of 600,000, the S825 and S809 airfoils' highest and lowest maximum C_L/C_D were 104.9 and 74.9, respectively. The S822, S823, S818, S814, S835, S821, and S828 airfoils' maximum C_L/C_D, respectively, were 101.4, 93.4, 91.8, 90.5, 81.9, 79.4, and 77.14. Therefore, the S825 airfoil's greatest maximum C_L/C_D was measured at Re of 100,000 to 600,000, whereas the S809 airfoil's lowest maximum C_L/C_D was measured at Re of 100,000, 200,000, 500,000, and 600,000. Additionally, at Re of 300,000 and 400,000, the S828 airfoil had the lowest maximum C_L/C_D.

Figure 2e shows a number of the Selig airfoils. The S1223 airfoil had the greatest maximum C_L/C_D of 52.47 at a Re of 100,000, while the S1046 airfoil had the lowest maximum C_L/C_D of 33.67. S4083, S7012, S8036, S8052, S5010, S6063, and S2027 airfoils had maximum C_L/C_D of 51.89, 51.1, 47.46, 47.33, 44.91, 42.58, and 42.54. At a Re of 200,000, the S4083 and S6063 airfoils recorded the maximum C_L/C_D with values of 74.28 and 49.18, respectively. For the S1223, S8036, S7012, S2027, S8052, S5010, and S1046 airfoils, the maximum C_L/C_D were 71.18, 69.75, 69.36, 65.36, 64.3, and 54.67, respectively.

The highest and lowest maximum C_L/C_D were measured at Re of 300,000, S4083, and S6063, respectively, and they were 86.55 and 49.78. The maximum C_L/C_D of the airfoils for the S2027, S1223, S7012, S8036, S5010, S8052, and S1046 were equal to 83.57, 82.66, 78.52, 77.87, 73.46, 72.97, and 64.78. The greatest and lowest maximum C_L/C_D for S4083 and S6063 airfoils were 95.96 and 51.5 at Re of 400,000, respectively. The maximum C_L/C_D for the airfoils S2027, S1223, S7012, S8036, S5010, S8052, and S1046 were 93.7, 92.1, 84.38, 83.59, 79.71, 78.35, and 70.9, respectively.

The greatest and lowest maximum C_L/C_D for the S2027 and S6063 airfoils were 102.43 and 55.5, respectively, at a Re of 500,000. S4083, S1223, S8036, S7012, S5010, S8052, and S1046 airfoils' maximum C_L/C_D were measured at 102.02, 98.3, 88.73, 86.55, 84.5, 82.24, and 74.6, respectively. Finally, at the Re of 600,000, the maximum

C_L/C_D for the S2027 and S6063 airfoils were 107.8 and 59.88, respectively. The S2027, S1223, S8036, S7012, S5010, S8052, and S1046 airfoils' greatest and lowest maximum C_L/C_D were measured at 107.8, 102.6, 92.7, 89.1, 88.69, 84.03, and 77.63, respectively.

Hence, the S1223 airfoil recorded the highest maximum C_L/C_D at a Re of 100,000. Additionally, with a Re of 200,000 to 300,000, the S4083 airfoil had the highest maximum C_L/C_D. The S2027 airfoil had the highest maximum C_L/C_D at Re of 400,000 to 600,000, whereas the S1046 airfoil achieved the lowest maximum C_L/C_D at Re of 100,000. Additionally, the S6063 airfoil had the lowest maximum C_L/C_D at Re of 200,000 to 600,000.

A number of Selig airfoils are displayed in **Figure 2f**. The SD2030 airfoil had the highest maximum C_L/C_D of 56.07 at Re of 100,000, whereas the SD7003 airfoil had the lowest maximum C_L/C_D of 43.12. For the airfoils SA7038, SD7032, SD7037, SA7035, SD7080, SD6060, and SD7062, the maximum C_L/C_D were 55.75, 55.33, 54.56, 52.57, 52.03, 49.78, and 44.6, respectively. At a Re of 200,000, the SD7032 and SD7003 airfoils obtained the highest and lowest maximum C_L/C_D, respectively, at 78.21 and 57.87.

For the SA7038, SD2030, SD7037, SA7035, SD7080, SD7062, and SD6060 airfoils, the maximum C_L/C_D were 77.06, 76.67, 74.78, 71.37, 70.19, 69.89, and 69.44, respectively. The highest and lowest maximum C_L/C_D were measured at Re of 300,000, SD7032, and SD7003, respectively, and they were 91.65 and 66.44. The respective values are 88.53, 88.17, 85.86, 84.04, 82.64, 81.24, and 80.20 for the SA7038, SD2030, SD7037, SD7062, SA7035, SD6060, and SD7080 airfoils.

The greatest and lowest maximum C_L/C_D for the SD7032 and SD7003 airfoils were 100.08 and 74.03 at a Re of 400,000, respectively. The maximum C_L/C_D for the airfoils SD2030, SA7038, SD7037, SD7062, SA7035, SD6060, and SD7080 were 97.39, 97.24, 94.68, 92.43, 90.27, 87.6, and 85.49, respectively. The highest and lowest maximum C_L/C_D for the SD7032 and SD7003 airfoils were 107.39 and 78.49, respectively, at a Re of 500,000. The SD2030, SA7038, SD7062, SD7037, SA7035, SD6060, and SD7080 airfoils' maximum C_L/C_D were measured at 103.46, 103.17, 101.47, 98.63, 95.46, 93.53, and 89.08, respectively.

In the end, at the Re of 600,000, the highest and lowest maximum C_L/C_D for the SD7032 and SD7003 airfoils were 112.87 and 82.36, respectively. The SD7062, SA7038, SD2030, SD7037, SA7035, SD6060, and SD7080 airfoils' maximum C_L/C_D were measured at 107.93, 107.52, 106.66, 102.07, 100.37, 97.78, and 94.16, respectively. Thus, the SD2030's highest maximum C_L/C_D was recorded at Re of 100,000, and the SD7032's was recorded at Re of 200,000 to 600,000. Furthermore, at Re between 100,000 and 600,000, the SD7003 airfoil had the lowest maximum C_L/C_D.

The SG6040, SG6041, SG6042, SG6043, SG6050, SG605, PSU94-097, and RG15 airfoils are depicted in **Figure 2g**. At Re of 100,000, the SG6043 airfoil had the highest maximum C_L/C_D, measuring 65.68, and the SG6050 airfoil had the lowest maximum, measuring 48.19. For the airfoils PSU94-097, SG6051, SG6041, RG15, and SG6040, the maximum C_L/C_D were 63.15, 59.3, 55.57, 53.4, 51.81, and 51.03, respectively. The highest and lowest maximum C_L/C_D were obtained by the SG6043 and SG15 airfoils at 97.21 and 68.9, respectively, at a Re of 200,000.

PSU94-097, SG6042, SG6051, SG6050, SG6040, and SG6041 airfoils' the greatest and lowest maximum C_L/C_D were 90.47, 89.01, 80.61, 73.89, 72.85, and 72.5, respectively. The maximum C_L/C_D for the SG6043 and RG15 airfoils at Re of 300,000 were 117.41 and 78.3, respectively. The maximum C_L/C_D airfoils for the PSU94-097, SG6042, SG6051, SG6050, SG6040, and SG6041 were equal to 106.92, 105.09, 95.7, 88.81, 83.82, and 82.61. The highest and lowest maximum C_L/C_D for the SG6043 and RG15 airfoils were 132.89 and 84.88, respectively, at a Re of 400,000. The maximum C_L/C_D for the PSU94-097, SG6042, SG6051, SG6050, SG6040, and SG6041 airfoils was 119.08, 115.78, 104.48, 98.63, 92.17, and 88.34, respectively.

The highest and lowest maximum C_L/C_D for the SG6043 and RG15 airfoils were 143.47 and 89.99, respectively, at a Re of 500,000. The PSU94-097, SG6042, SG6051, SG6050, SG6040, and SG6041 airfoils had the maximum C_L/C_D of 126.1, 123.77, 113.62, 106.16, 97.84, and 91.14, respectively. Finally, at a Re of 600,000, the highest and lowest maximum C_L/C_D for the SG6043 and RG15 airfoils were 153.09 and 92.5, respectively. The PSU94-097, SG6042, SG6051, SG6050, SG6040, and SG6041 airfoils had a maximum C_L/C_D of 135.1, 131.19, 119.59, 111.67, 103.2, and 93.4, respectively. The SG6043 airfoil had the highest maximum C_L/C_D, which was measured at Re of 100,000 to 600,000, while the SG6050 airfoil had the lowest maximum C_L/C_D, measured at Re of 100,000, and the RG15 airfoil at Re of 200,000 to 600,000.

The E231, USNPS4, E387, BW-3, E374, ESA40, E423, FX63-137, and FX74-Cl5-140 airfoils are depicted in **Figure 2h**. The BW-3 airfoil had the highest maximum C_L/C_D of 58.7 at a Re of 100,000, while the E423 airfoil had the lowest maximum C_L/C_D of 12.94. Respectively, the maximum C_L/C_D for E387, USNPS4, FX63-137, E374, E231, FX74-Cl5-140, and ESA40 airfoils were 57.19, 54.93, 54.42, 53.02, 52.77, 33.09, and 24.17.

At a Re of 200,000, the FX63-137 and ESA40 airfoils obtained the highest and lowest maximum C_L/C_D, respectively, at 90.29 and 37.04. E387, E231, USNPS4, E374, FX74-Cl5-140, BW-3, and E423 airfoils had maximum C_L/C_D that were, respectively, 81.97, 76.84, 74, 73.31, 72.74, and 72.04 and 60.75. The highest and lowest maximum C_L/C_D were measured at Re of 300,000 for the FX63-137 and ESA airfoils, respectively, at 107.31 and 50.36. The E387, FX74-Cl5-140, E423, E231, USNPS4, E374, and BW-3 airfoils were equal to 93.82, 93.33, 91.08, 88, 84.79, 84.47, and 75.4, respectively.

At a Re of 400,000, the highest and lowest maximum C_L/C_D for the FX63-137 and ESA40 airfoils were 119.4 and 60.24, respectively. The maximum C_L/C_D for the airfoils E423, FX74-Cl5-140, E387, E374, USNPS4, E231, and BW-3 were 109.46, 108, 99.95, 94.17, 91.27, 91, and 78.03, respectively. The greatest and lowest maximum C_L/C_D for the FX63-137 and EAS40 airfoils at Re of 500,000 were 129.64 and 67.72, respectively. The E423, FX74-Cl5-140, E387, E374, USNP4, E231, and BW-3 airfoils' maximum C_L/C_D was measured at 122.94, 119.16, 106, 97.47, 95.38, 94.05, and 84.31, respectively.

Finally, at the Re of 600,000, the highest and lowest maximum C_L/C_D for the FX63-137 and ESA40 airfoils were 135.28 and 73.3, respectively. The E423, FX74-Cl5-140, E387, E374, USNPS4, E231, and BW-3 airfoils' maximum C_L/C_D were measured at 132.9, 129.12, 109.2, 103.1, 99.94, 94.5, and 87.6, respectively. The BW-

3 airfoil's highest maximum C_L/C_D was measured at Re of 100,000, and the FX63-137's was between Re 200,000 to 600,000. Additionally, the E423 airfoil at Re of 100,000 and the ESA40 airfoil at Re of 200,000 to 600,000 achieved the lowest maximum C_L/C_D.

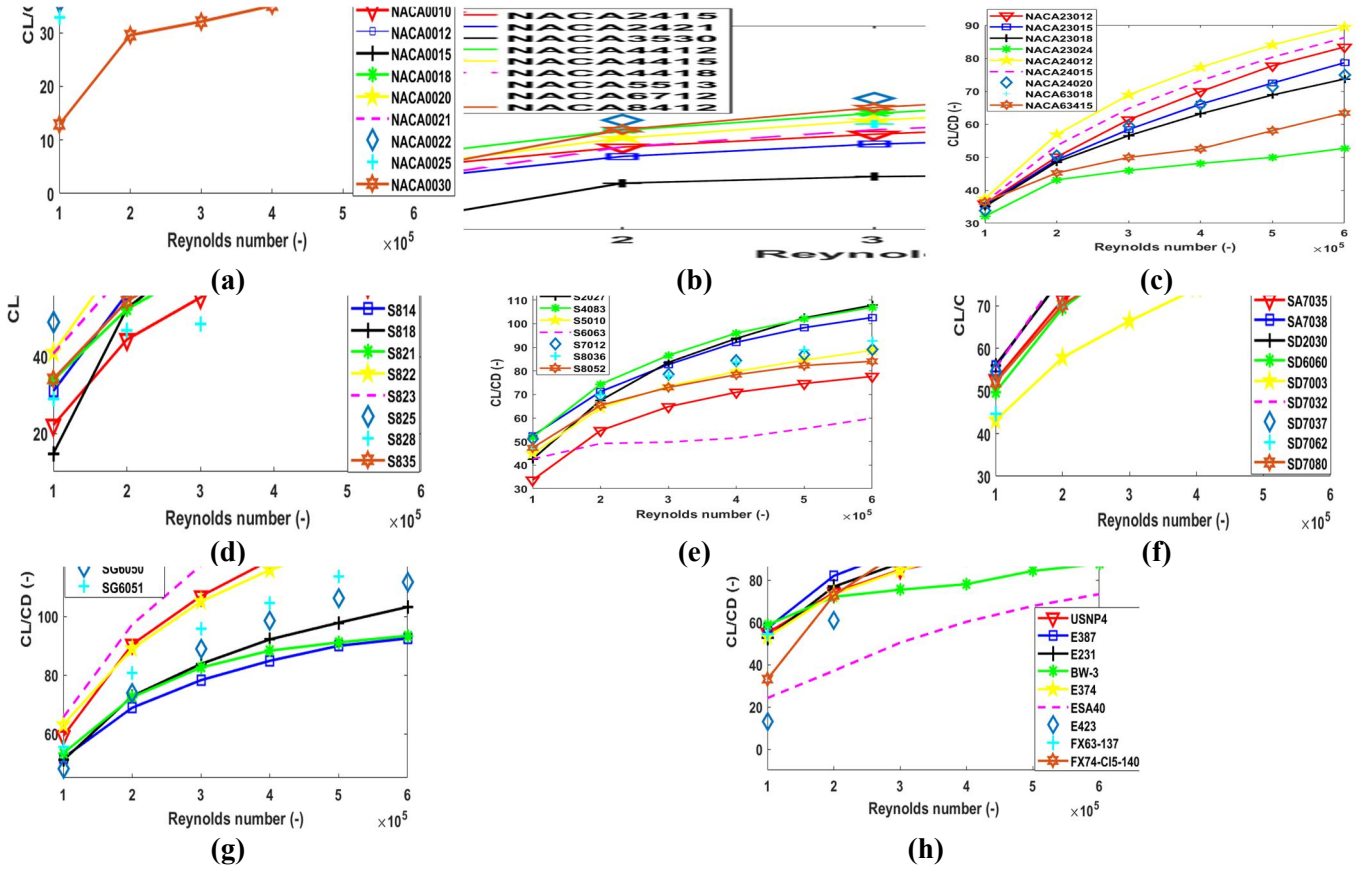

Figure 2. Analyzing the maximum C_L/C_D of selected airfoils at Reynolds numbers (Re) ranging from 100,000 to 600,000. **(a)** Symmetrical NACA 4-digit airfoils; **(b)** other NACA 4-digit airfoils; **(c)** NACA 5-digit airfoils; **(d)** Selig airfoils (3-digit); **(e)** Selig airfoils (4-digit); **(f)** Selig airfoils (SA/SD series); **(g)** SG604x and related airfoils; **(h)** Eppler and other airfoils.

As a consequence, the SG6043 airfoil revealed the highest maximum C_L/C_D when compared to the other 71 airfoils evaluated at Re from 100,000 to 600,000. To investigate and enhance the form modification of the airfoil utilizing variations in *t*/*c* and to determine the ideal *t*/*c* at Re of 10,000 to 600,000, the SG6043 airfoil was used. We can develop another airfoil by modifying the shape variations in the *t*/*c* using the XFOIL software. At each *t*/*c* configuration, research was carried out on the most suitable new airfoil for optimum C_L/C_D at Re ranging from 10^5 to 6×10^5. Then, utilizing the zone of *t*/*c* with the more significant value C_L/C_D, the geometrical parameters of the SG6043 modified airfoils were found.

Aerodynamic efficiency metrics for the novelty-modified airfoils, including C_L, C_D, C_L/C_D, AoA_{stall}, and drag buckets, were determined and investigated with the baseline airfoil at a Re of 10^5 to 6×10^5 and for the *AoA* range from 0° to 20°. A summary of the procedure used for the novel airfoil under investigation in XFOIL software is shown in **Figure 3a**.

Turbine blades are critical components in converting fluid or gas energy into mechanical energy. Optimizing their shape, material, and design enhances aerodynamic efficiency, reducing energy losses and improving overall turbine performance. As well better efficiency translates to higher power output for the same input energy, which is particularly important in power plants and aircraft engines. The optimization process of XFOIL is shown in **Figure 3b**. The effectiveness standards for innovative airfoils were changed, and Section 3 presents the effective methods. simplified version of the XFOIL optimization flowchart is shown in Algorithm 1 as below:

Algorithm 1 Airfoil optimization

```
Start
Define Airfoil Geometry
  - Input initial airfoil shape parameters.
Set Flow Conditions
  - Specify Reynolds number, Mach number, and angle of attack.
Run XFOIL Analysis
  - Compute lift, drag, and moment coefficients.
Evaluate Performance
  - Check if the performance meets the desired criteria.
Optimization Loop
  - If not optimized:
    - Modify airfoil shape using optimization algorithm.
    - Return to step 3.
  - If optimized:
    - Proceed to next step.
Output Optimized Airfoil
  - Save the final airfoil geometry and performance data.
End
```

This is a high-level overview. The actual process can be more complex depending on the specific optimization algorithms and criteria used.

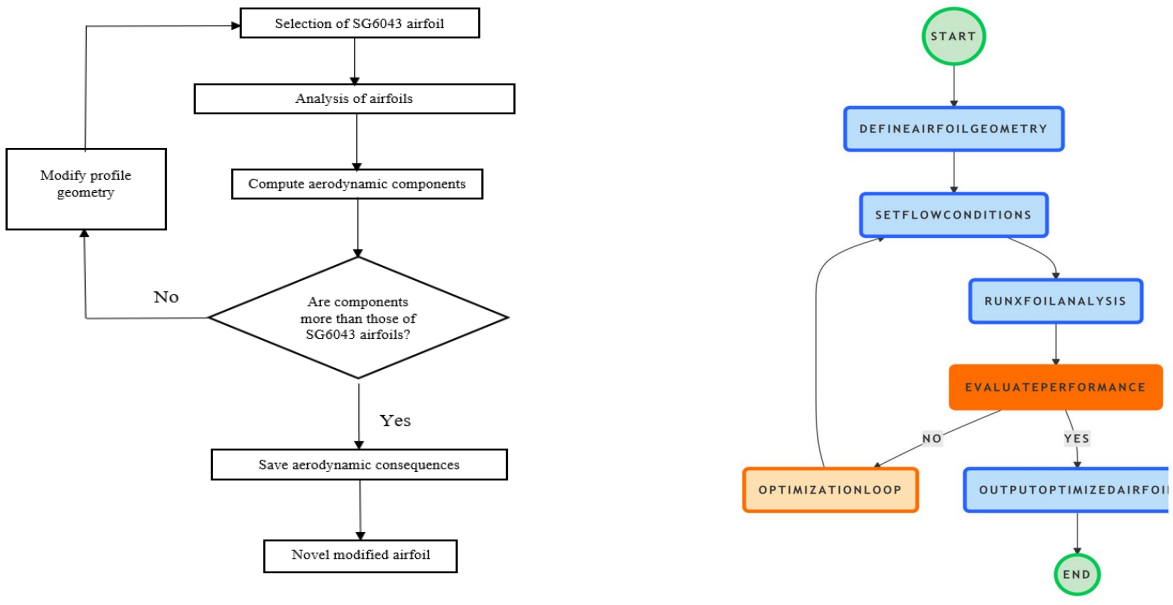

(a) **(b)**

Figure 3. (a) Abstract of XFOIL software process for profile experiment; **(b)** optimization process.

2.3. Theoretical framework

The SG6043 airfoil was modified by varying the thickness-to-camber ratio (*t*/*c*) between 0.5 and 1.5. Three modified airfoils (SG6043 modified 1, 2, and 3) were designed and analyzed to determine their aerodynamic performance. Equations (1)–(5) show the mathematical basis for investigating the aerodynamic characteristics of the airfoil [25,26].

$$Reynoldsnumber = \frac{\rho U_{rel} c}{\mu} = \frac{U_{rel} c}{\upsilon} \tag{1}$$

$$U_{rel} = \sqrt{[U(1-a)]^2 + [r\omega]^2} \tag{2}$$

$$L = C_l \frac{1}{2} \rho U^2 cl \tag{3}$$

$$D = C_d \frac{1}{2} \rho U^2 cl \tag{4}$$

$$\frac{L}{D} = \frac{(C_l \frac{1}{2} \rho U^2 cl)}{(C_d \frac{1}{2} \rho U^2 cl)} = \frac{C_l}{C_d} \tag{5}$$

Equation (1) defines a relationship between the speed of air, kinematic viscosity, airfoil chord length, and wind Re. The lift force (F_L) and drag force (F_D) of an airfoil can be calculated in Equations (3) and (4), respectively.

Equation (3) illustrates the relationship between the F_L and the C_L by including the air speed, density, chord length, and span. In Equation (4), the F_D on the airfoil is correlated with the C_D, speed of the wind, density, chord, and span. The C_L/C_D was provided by Equation (5).

2.4. SG6043 airfoil modified optimization

Based on initial design optimization findings, **Figure 4a** illustrates variations in reaching their highest C_L/C_D with *t*/*c* for the SG6043 airfoil for Re from 10^5 to 6×10^5. **Figure 4a** shows that the peak C_L/C_D had a dome-shaped relationship with the *t*/*c* for each Re, and that the efficiency of C_L/C_D generally improved with rising Re. The maximum peak CL/CD occurred within the *t*/*c* range of 0.50 to 1.50 for each Re. Hence, the top C_L/C_D was smaller outside of this *t*/*c* range. The *t*/*c* of the SG6043 airfoil was determined using the *t*/*c*, which was considered when generating the airfoils in the current research. The *t*/*c* ranged from 0.50 to 1.50.

SG6043 modified 1 airfoil was optimized to have a pick thickness of 7.05% at 17.20% of the chord and a pick camber of 7.72% at 49.80% of the chord, SG6043 modified 2 airfoils was optimized to have a pick thickness of 6.52% at 15.30% of the chord and a pick camber of 8.79% at 53.20% of the chord; and SG6043 modified 3 airfoils was optimized to have a pick thickness of 4.91% at 15.70% of the chord and a pick camber of 8.88% at 52.50% of the chord, as was represented graphically in **Figure 4b**. Moreover, the SG6043 airfoil had a peak thickness of 10.02% at 32.10% of the chord and a peak camber of 5.50% at 49.70% of the chord.

Hence, the *t*/*c* range for these parameters was between 0.50 and 1.50. This zone saw the development of three airfoils with the designations SG6043 modified 1, SG6043 modified 2, and SG6043 modified 3. According to **Figure 4b**, the significant variation between the SG6043 airfoil and the novelty-modified SG6043 modified airfoils was in the geometrical features of the thickness and camber airfoils. In comparison to the SG6043 airfoil, the SG6043 modified airfoils had thinner and more cambered geometries. As previously mentioned, the efficiency parameters of the novelty-designed airfoils and the SG6043 airfoil were calculated at a Re of 10^5 to 6×10^5.

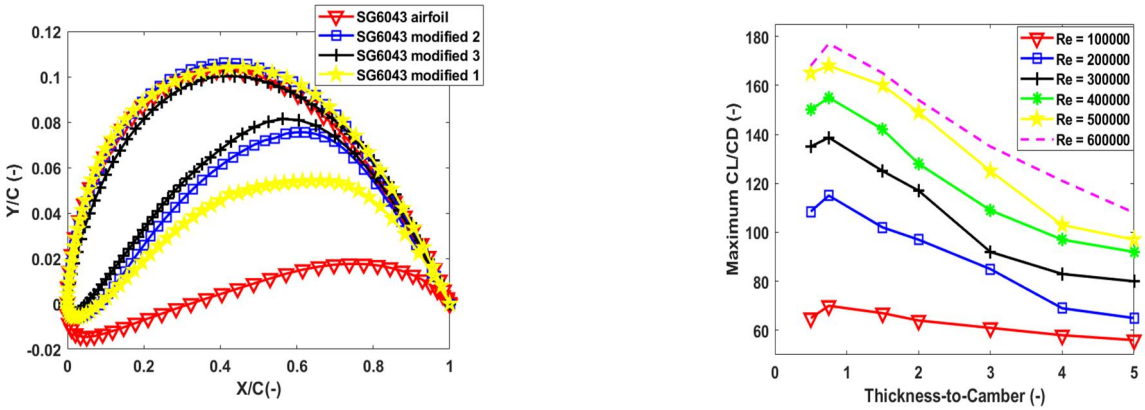

(a) **(b)**

Figure 4. Airfoil geometry variation for SG6043 airfoil optimization, **(a)** peak C_L/C_D at various thickness-to-camber ratios; **(b)** SG6043 and SG6043 modified airfoils.

3. Results and discussions

3.1. Validation data

As illustrated in **Figure 5a**,**b**, which compare the aerodynamic efficiency of the E387 airfoil as predicted by X-Foil at Re of 200,000 and 400,000 with the experiment and X-Foil data by Wei et al. [27] in order to confirm the correctness of the X-Foil software. The results from the experiment and X-Foil software are in strong agreement with one another, which can support the need for optimization.

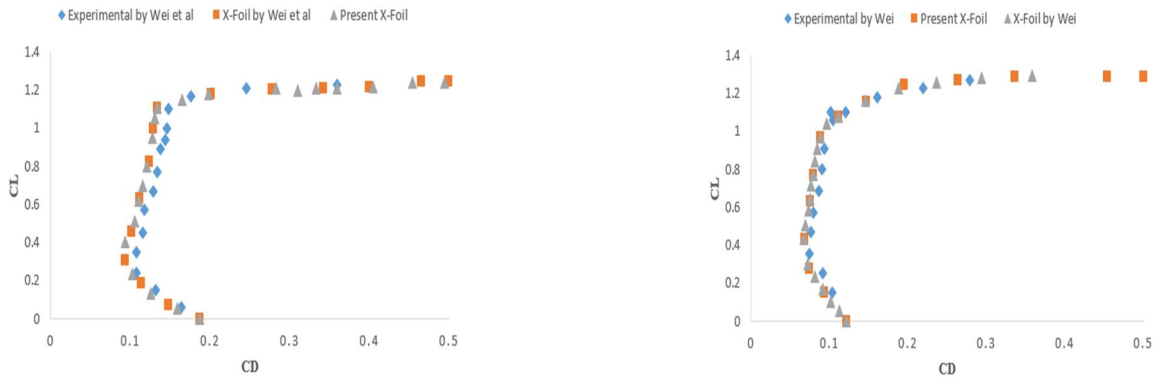

(a) **(b)**

Figure 5. Variation of aerodynamic parameters predicted by the XFOIL software data and experimental findings [27]. (**a**) Re = 200,000, (**b**) Re = 400,000.

3.2. Lift efficiency of SG6043, SG6043 modified 1, SG6043 modified 2, and SG6043 modified 3 airfoils

For Re between 100,000 and 600,000, the lift efficiency graphs for the base and modified SG6043 modified 1, SG6043 modified 2, and SG6043 modified 3 airfoils were illustrated in **Figures 6–9**, respectively. The value of the C_L had increased for the SG6043 airfoil as the Re had risen from 10^5 to 6×10^5; the lowest value of the C_L in the Re of 10^5 was equal to 1.604, and the highest value of the C_L in the Re of 6×10^5 was 1.769 (**Figure 6**).

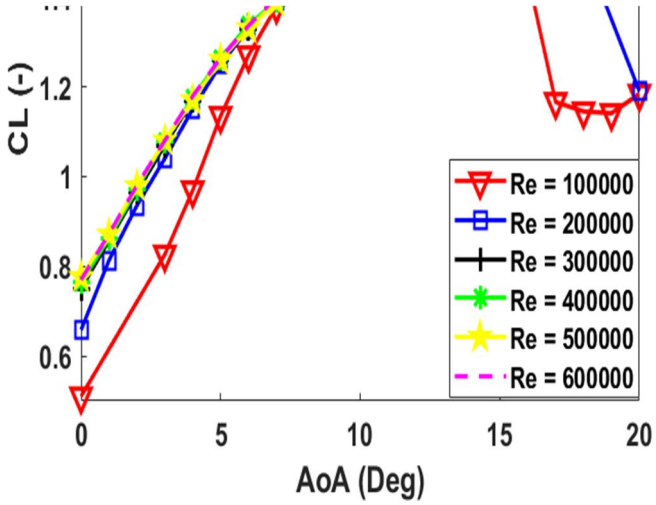

Figure 6. C_L graph for SG6043 airfoil.

The SG6043 modified 1 airfoil had the greatest peak C_L of 1.79 at a Re of 10^5. The lowest peak C_L of 1.72 equaled a Re of 3×10^5. The findings demonstrated that when the Re increased, C_L generally increased better. SG6043 modified 1 had near lift efficiency for Re between 2×10^5 and 5×10^5. Moreover, the C_L at Re of 3×10^5, 4×10^5, 5×10^5, and 6×10^5 equal to 1.72, 1.74, 1.75, and 1.772, respectively. This value had risen as Re from 3×10^5 to 6×10^5 had increased (**Figure 7**).

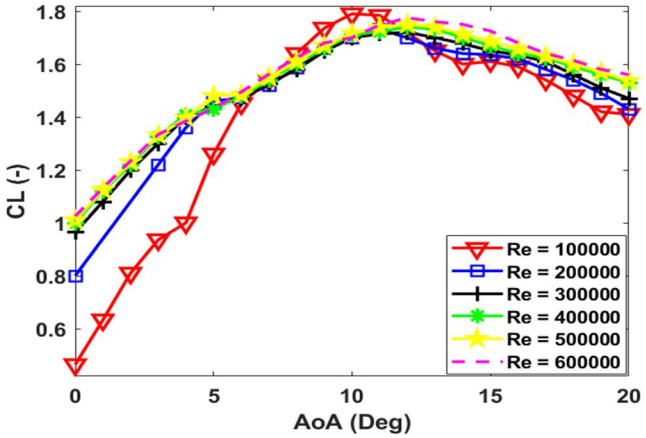

Figure 7. C_L graph for SG6043 modified 1 airfoil.

Figure 8 illustrates the lift efficiency graph for the SG6043 modified 2 airfoils at Re between 10^5 to 6×10^5. Similarly, as Re increased, C_L efficiency generally

improved. For *AoAs* less than 12° at Re of 10^5 to 6×10^5, the C_L efficiency was close to each other. At Re of 6×10^5 and 2×10^5, the SG6043 modified 2 airfoil had peaks C_L of 1.798 and 1.743, respectively, the most excellent and lowest values. Also, at a Re of 10^5, the greatest value of the C_L was equal to 1.748, which was more than a Re of 2×10^5 and less than a Re of 3×10^5 to 6×10^5.

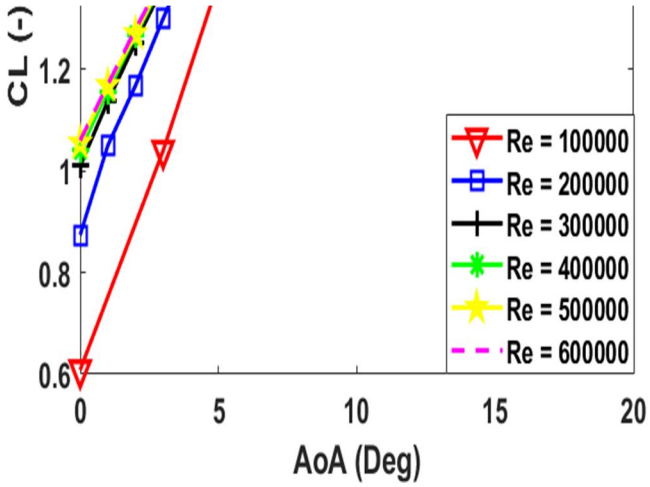

Figure 8. C_L graph for SG6043 modified 2 airfoil.

The lift efficiency graph for SG6043 modified 3 airfoils with a Re of 10^5 to 6×10^5 is indicated in **Figure 9**. The C_L efficiency was enhanced with an increment in Re, with relative efficiency for Re of 2×10^5, 3×10^5, 5×10^5, and 6×10^5. The SG6043 modified 3 airfoil had the greatest and least peak C_L of 1.788 and 1.697, respectively, at Re of 10^5 and a Re of 4×10^5, respectively. In addition, the peak C_L in Re of 2×10^5, 3×10^5, 5×10^5, and 6×10^5 equals 1.763, 1.781, 1.773, and 1.778.

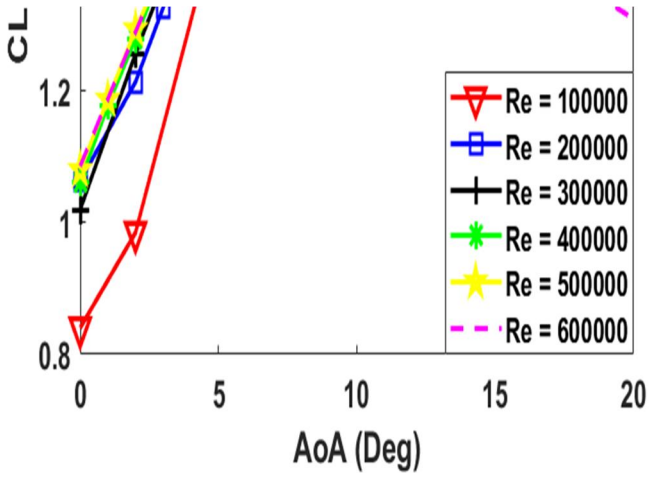

Figure 9. C_L graph for SG6043 modified 3 airfoil.

Typically, the peak C_L of modified airfoils in all Re was greater than the peak C_L of the SG6043 airfoil, and the enhancement in lift efficiency for an increment in Re was related to an incremented air velocity relevant to a higher Re.

Moreover, at each Re, the decrement in lift efficiency beyond the peak C_L was related to the airfoils encountering stall situations as a consequence of lift resistance from turbulence on the airfoil's suction surfaces. At a Re of 3×10^5, there was almost

no discernible difference in lift efficiency between any airfoil. This near-efficiency attitude indicates that the lift efficiency of the airfoils was comparatively less susceptible to changes in Re from Re of 3×10^5 to 6×10^5. This effect was related to nonlinear aerodynamic properties frequently found in low Re airflow situations [28].

3.3. Stall efficiency of SG6043 modified 1, SG6043 modified 2, and SG6043 modified 3 airfoils

The stall efficiency of SG6043 modified 1, SG6043 modified 2, and SG6043 modified 3 airfoils at Re from 10^5 to 6×10^5 was investigated in **Table 1**. For the analysis, Re of 10^5 to 6×10^5, entire airfoils had AoA_{stall} between 9° to 13°.

Table 1. Stall performances for SG6043 modified airfoils.

Airfoils	**Stall Angle (°)**					
	Re = 10^5	**Re = 2×10^5**	**Re = 3×10^5**	**Re = 4×10^5**	**Re = 5×10^5**	**Re = 6×10^5**
SG6043 modified 1	10	11	12	12	12	12
SG6043 modified 2	12	12	13	13	13	13
SG6043 modified 3	9	10.5	10	11	9	9

SG6043 modified 1 airfoil had the lowest AoA_{stall} of 10° at Re of 10^5 and the greatest AoA_{stall} of 12° at Re of 3×10^5, 4×10^5, 5×10^5, and 6×10^5. Moreover, AoA_{stall} of 11° was presented at a Re of 2×10^5. The SG6043 modified 2 airfoil had the least AoA_{stall} of 12° at Re of 10^5 and 2×10^5. Moreover, SG6043 modified 2 airfoils had the most excellent AoA_{stall} of 13° at Re of 3×10^5, 4×10^5, 5×10^5, and 6×10^5, respectively.

The SG6043 modified 3 airfoil had the least AoA_{stall} of 9° at Re of 10^5, 5×10^5, and 6×10^5. Also, SG6043 modified 3 airfoils had the most significant AoA_{stall} of 11° at Re of 4×10^5. As well as, AoA_{stall} of 10.5° and 10° were presented at Re of 2×10^5 and 3×10^5. The AoA_{stall} demonstrates the crucial AoA beyond which the C_L efficiency starts to degrade due to resistance generated by turbulence on the airfoil's suction area for every airfoil under each Re flow regime.

The greatest AoA_{stall} of 13º and 12º for SG6043 modified 2 airfoil for nearly the entire Re demonstrated it was favorable for utilization over and across a comparatively wider AoA.

Figures 7–9's lift efficiency graphs showed that total airfoils often produced post-stall slow performance at Re of 200,000. The shape of the airfoils, which was developed for the most incredible C_L/C_D efficiency and was required for continuous aerodynamic efficiency at an extensive range of AoA without a short loss of lift, causes this slow post-stall feature. It was known that abrupt lift loss causes WT rotor efficiency to degrade quickly [28].

3.4. The C_L/C_D efficiency of SG6043 and SG6043 modified airfoils

The SG6043 modified 1 airfoil demonstrated the highest lift coefficient (C_L) of 1.79 at Re = 100,000, outperforming the original SG6043 airfoil. As Re increased, the C_L for all modified airfoils improved, with the SG6043 modified 2 airfoil achieving a peak C_L of 1.798 at Re = 600,000 (**Figure 6**). This improvement in lift efficiency is

attributed to the optimized *t*/*c* ratio, which enhances airflow over the airfoil surface. The C_L/C_D efficiency graphs of SG6043, SG6043 modified 1, SG6043 modified 2, and SG6043 modified 3 airfoils for Re of 10^5 to 6×10^5 were illustrated in **Figures 10**–**13**, respectively. The C_L/C_D efficiency typically increased with increasing Re for airfoils and had a dome-shaped relationship with *AoA* for the entire Re. Throughout the whole *AoA*, the C_L/C_D efficiency was greatest at a Re of 6×10^5 and lowest at a Re of 10^5. According to **Figure 10**, at a Re of 6×10^5, the SG6043 airfoil's greatest peak C_L/C_D was 152.88 at an *AoA* of 3°. The least peak C_L/C_D at Re of 10^5 was 65.86 at an *AoA* of 7°. The highest C_L/C_D for the SG6043 airfoil was 97.21, 117.25, 132.5, and 143.33, respectively, for Re of 2×10^5, 3×10^5, 4×10^5, and 5×10^5, at *AoA* of 5°, 4°, 4°, and 3°.

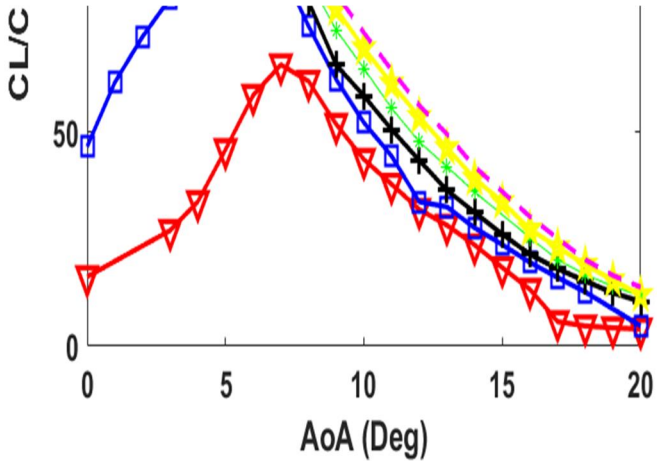

Figure 10. The C_L/C_D efficiency for SG6043 airfoil.

From **Figure 11**, at a Re of 6×10^5, the highest peak C_L/C_D for the SG6043 modified 1 airfoil was 184.85 at $AoA = 3°$. At a Re of 10^5, the least peak C_L/C_D was 69.48 at $AoA = 6°$. At Re of 2×10^5, 3×10^5, 4×10^5, and 5×10^5, the greatest values C_L/C_D for SG6043 modified 1 airfoil were 108.47, 135.59, 154.3, and 172.43, respectively, at *AoAs* of 5°, 4°, 3°, and 3°.

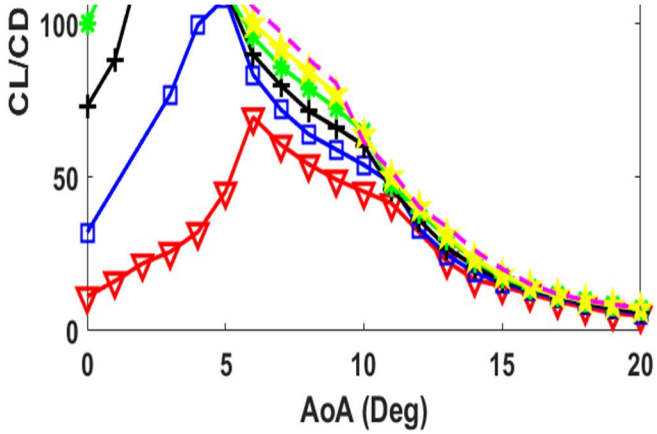

Figure 11. The C_L/C_D efficiency for SG6043 modified 1 airfoil.

From **Figure 12**, at a Re of 6×10^5, the greatest peak C_L/C_D for the SG6043 modified 1 airfoil was 177.25 at $AoA = 3°$. At a Re of 10^5, the least peak C_L/C_D was

73.08 at AoA = 7°. At Re of 2 × 10^5, 3 × 10^5, 4 × 10^5, and 5 × 10^5, the highest values of C_L/C_D for SG6043 modified 1 airfoil were 111.70, 138.67, 160.80, and 171.08, respectively, at $AoAs$ of 5°, 4°, 4°, and 4°.

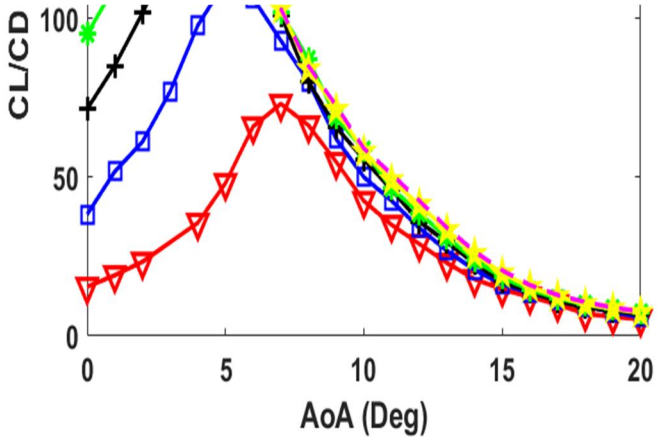

Figure 12. The C_L/C_D efficiency for SG6043 modified 2 airfoil.

According to **Figure 13**, at a Re of 6 × 10^5, the SG6043 modified 3 airfoil's greatest peak C_L/C_D was 182.36 at an AoA of 2°. The least peak C_L/C_D at a Re of 10^5 was 71.34 at an AoA of 6°. The highest C_L/C_D for the SG6043 modified 3 airfoil was 116.98, 145.02, 157.34, and 170.15, respectively, for Re of 2 × 10^5, 3 × 10^5, 4 × 10^5, and 5 × 10^5, at $AoAs$ of 4°, 3°, 3°, and 2°, respectively.

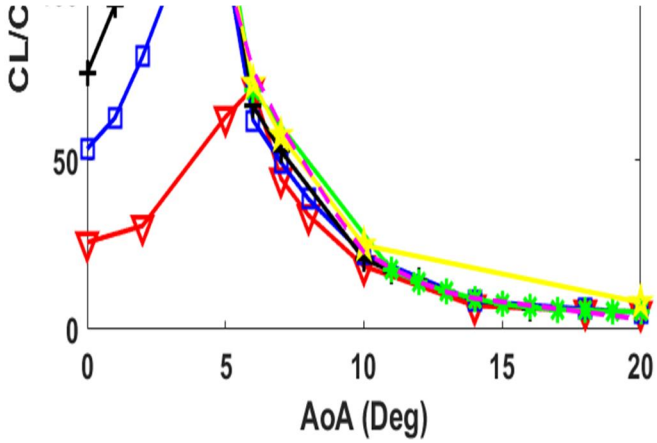

Figure 13. The C_L/C_D efficiency for SG6043 modified 3 airfoil.

The greatest C_L/C_D efficiency for each airfoil occurred at a Re of 6 × 10^5, which was related to a high energy flow and tried to produce a high lift. The maximum C_L/C_D efficiency for the SG6043 modified 1, SG6043 modified 2, and SG6043 modified 3 airfoils at Re of 3 × 10^5, respectively, was 135.59, 138.67, and 145.02, compared with further airfoils like the E387, SG6043, Go471a, and EYO-Series airfoils studied in other research [9,15,16,21].

3.5. Drag bucket performances of SG6043 and SG6043 modified airfoils

The SG6043 modified 2 airfoil exhibited the highest stall angle (AoA_{stall}) of 13° at Re = 300,000 to 600,000, making it suitable for a wider range of operating conditions (**Table 1**). This is a significant improvement over the original SG6043

airfoil, which had a stall angle of 12° at the same Re range. The drag bucket efficiency for the SG6043, SG6043 modified 1, SG6043 modified 2, and SG6043 modified 3 airfoils is shown in **Figures 14** and **15**, respectively. Typically, SG6043 and SG6043-modified airfoils had an increment in drag bucket efficiency with an incrementing Re. According to **Figure 14**, for the SG6043 airfoil and at a Re of 10^5, the first rise in the lift was accompanied by a slight decrease in drag up to a C_L of around 1.6. After this limit, there was a small drop in lift and a significant increase in drag. With no commensurate change in drag, the initial increment in C_L up to around 1.20 happened steadily at a Re of 6×10^5. Above C_L of 1.76, lift only was reduced while drag drastically increased. At Re of 2×10^5, 3×10^5, 4×10^5, and 5×10^5, there was a similar performance trend.

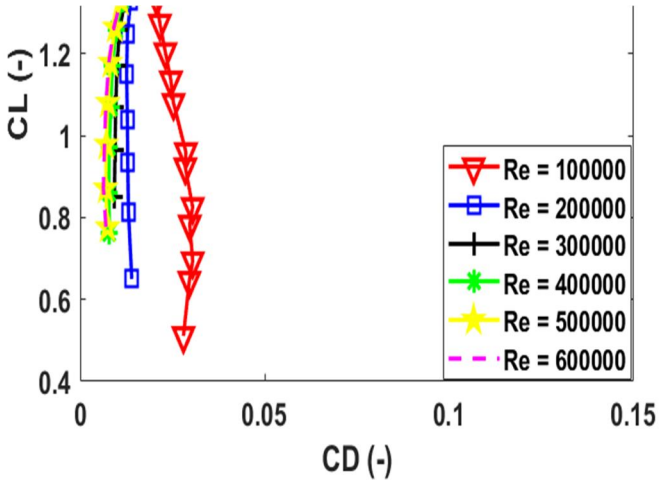

Figure 14. Drag bucket for SG6043 airfoil.

According to **Figure 15**, with the SG6043 modified 1 airfoil at a Re of 10^5, the primary rise in the lift was accompanied by a minor decrease in drag up to a C_L of around 1.78. After this amount, there was a slight drop in lift and a significant increase in drag. At a Re of 6×10^5, the C_L slowly increased at first, reaching a value of around 1.38, without any commensurate variation in drag. With only a modest reduction in lift, drag significantly rose above the C_L of 1.772. The efficiency trends for Re of 2×10^5, 3×10^5, 4×10^5, and 5×10^5 were comparable.

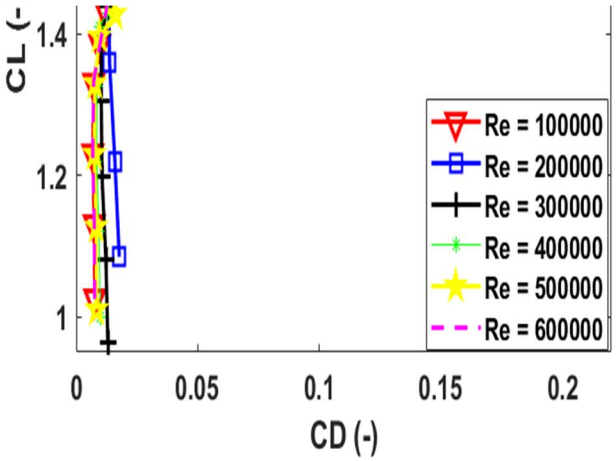

Figure 15. Drag bucket for SG6043 modified 1.

Figure 16 shows that for the SG6043 modified 2 airfoil at a Re of 10^5, the primary rise in the lift was accompanied by a minor decrease in drag up to a C_L of around 1.74. After this amount, there was a slight drop in lift and a significant increase in drag. At a Re of 6×10^5, the C_L slowly increased at first, reaching a value of around 1.53, without any commensurate variation in drag. With only a modest reduction in lift, drag significantly rose above the C_L of 1.798. The efficiency trends for Re of 2×10^5, 3×10^5, 4×10^5, and 5×10^5 were comparable.

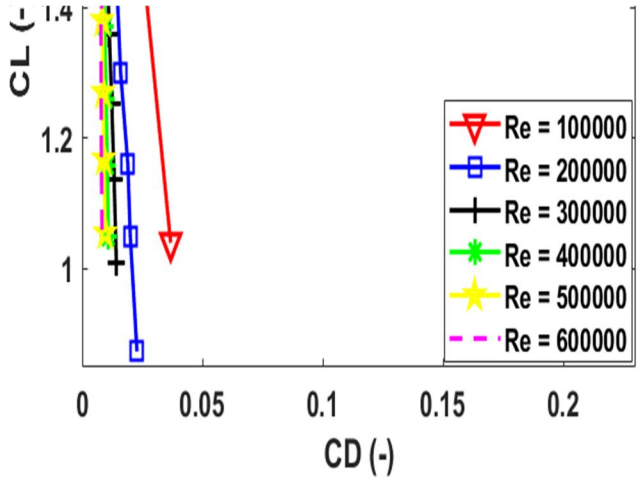

Figure 16. Drag bucket for SG6043 modified 2.

Figure 17 illustrates that with the SG6043 modified 3 airfoil at a Re of 10^5, the primary rise in the lift was accompanied by a minor decrease in drag up to a C_L of around 1.787. After this amount, there was a slight drop in lift and a significant increase in drag. At a Re of 6×10^5, the C_L slowly increased at first, reaching a value of around 1.47, without any commensurate variation in drag. With only a modest reduction in lift, drag significantly increased above the C_L of 1.778. The efficiency trends for Re of 2×10^5, 3×10^5, 4×10^5, and 5×10^5 were comparable.

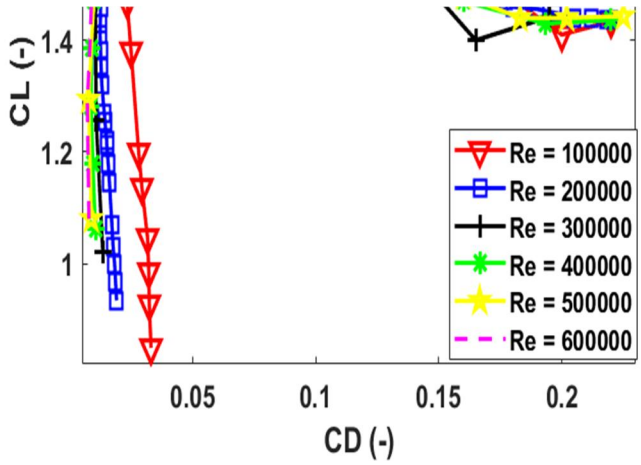

Figure 17. Drag bucket for SG6043 modified 3.

At the whole Re, every airfoil had its primary increment in C_L happening at either steady drag or decreasing drag up to around the region of peak C_L. This aerodynamic treatment resulted from how the airfoils were modified and developed for peak C_L/C_D

efficiency. The post-stall areas, where turbulence on the airfoil areas decreased lift generation and raised drag, include the area in the drag buckets beyond the peak C_L where the C_D incremented rapidly. The capability of the airfoils to increment lift efficiency to around the part of peak C_L while stabilizing or decreasing the surface of drag was a typically favorable feature of great-efficiency airfoils. All modified airfoils showed improved drag bucket performance, with the SG6043 modified 1 airfoil demonstrating the most significant reduction in drag at higher lift coefficients (**Figure 14**). This indicates that the modified airfoils are more efficient at maintaining lift while minimizing drag, which is critical for SWT performance.

3.6. Pressure distribution (C_P) of SG6043 modified airfoils

Figures 18–21 were illustrated, respectively, the upper and bottom surfaces C_P of the SG6043 modified 1, SG6043 modified 2, and SG6043 modified 3 airfoils at Re of 3×10^5 for the *AoA* of 0°, the angle at peak C_L/C_D, AoA_{stall}, and 20°. According to **Figure 18**, the modified airfoil had considerably bigger suction (negative pressures) on its upper area than on its bottom area at an *AoA* of 0°. Each airfoil's pressure loading along its chord length was almost consistent from the leading edge to the trailing edge. Due to the consistent pressure loading, it was possible to determine that the lift generated by the airfoils at an *AoA* of 0° was distributed uniformly from the leading to the trailing edges. For entire modified airfoils, the stagnation points (point of peak pressure) at an *AoA* of 0° were recorded at the leading edge.

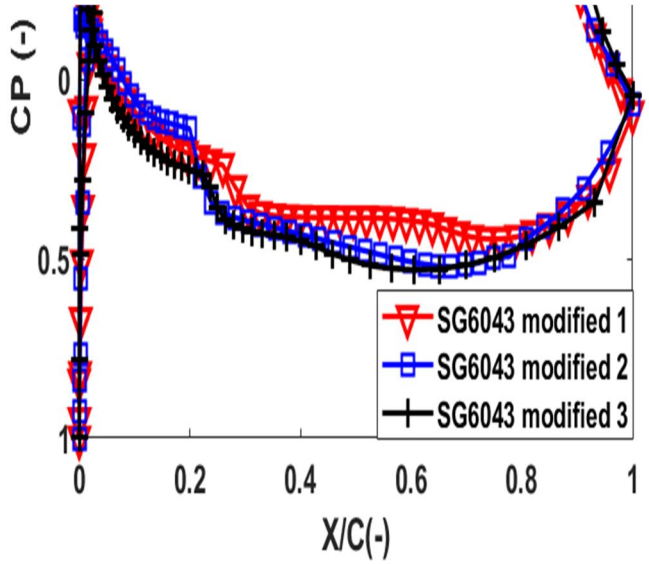

Figure 18. C_P of entire modified airfoils at an angle of attack of 0°.

According to **Figure 19**, a higher suction value on the upper area of all modified airfoils was localized towards the leading edge at the angle at peak C_L/C_D. Moreover, the pressure loading was higher towards the modified airfoils leading edge than their trailing edge. The results demonstrated that the surface immediately adjacent to the leading edge was primarily responsible for the lift efficiency of the airfoils at the angle at peak C_L/C_D. Leading edges were recorded as stagnation points for entire airfoils at angles at peak C_L/C_D.

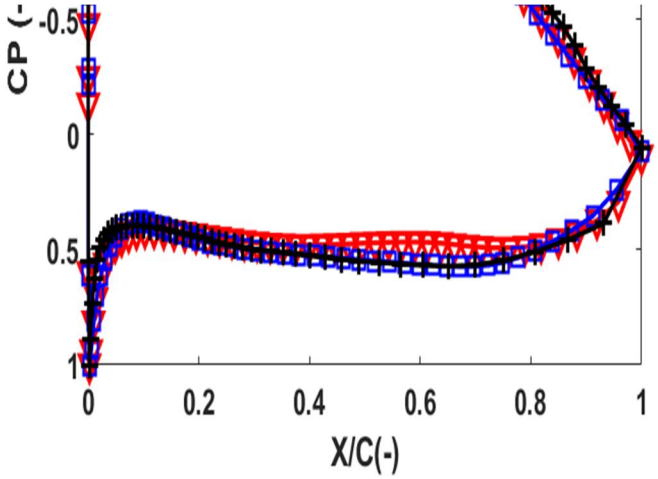

Figure 19. C_P of whole modified airfoils angle at peak C_L/C_D.

According to **Figures 20** and **21** for modified airfoils, the pressure loading was noticeably higher at the leading edge at an AoA_{stall} and an AoA of 20°, respectively. That demonstrated that the area closely adjacent to the leading edge contributed significantly to the lift efficiency of the airfoils at an AoA of 20°. For all the modified airfoils at both AoA investigated in **Figures 20** and **21**, the stagnation point was about 1% of the chord below the leading edge.

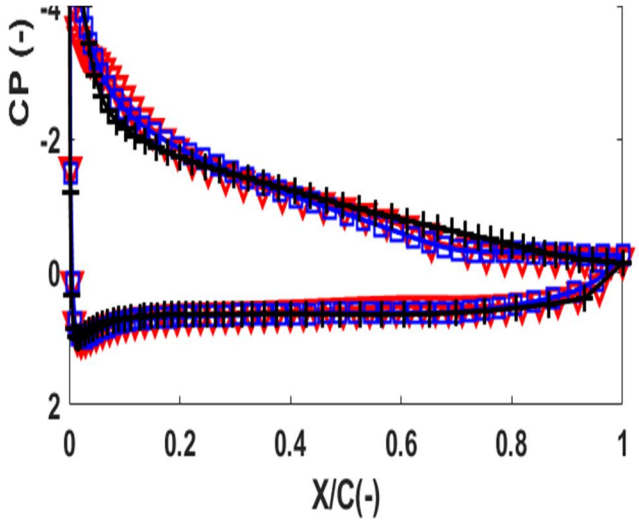

Figure 20. C_P of entire modified airfoils at AoA_{stall}.

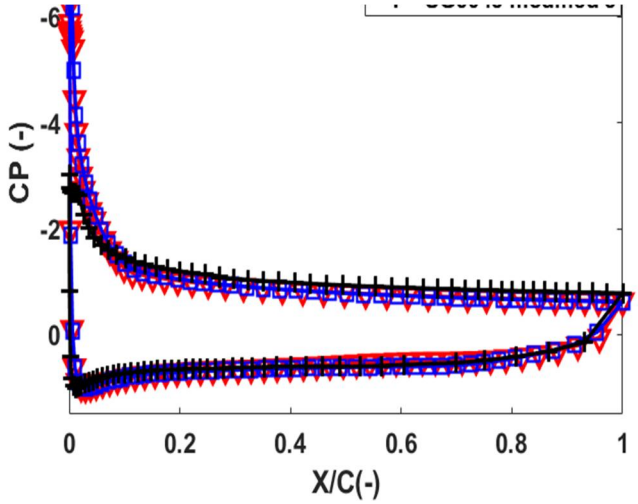

Figure 21. C_P of entire modified airfoils at an angle of attack of 20°.

On the low-pressure sides or top areas of the airfoils, greater F_L was typically correlated with a comparably more significant suction value. Consequently, the high C_L/C_D efficiency findings at that AoA were confirmed by the relatively wide suction pressure in the C_P data for the modified airfoils at an AoA of 4°.

4. Summary of performance analysis for modified airfoils

The C_L and C_L/C_D summary for the SG6043 modified 1, SG6043 modified 2, and SG6043 modified 3 airfoils were revealed in **Figures 22** and **23**, respectively. From **Figure 22**, the SG6043 modified 1 airfoil had the greatest peak C_L at the investigated Re of 10^5, while the SG6043 modified 2 airfoil had the lowest peak C_L. Plus, SG6043 modified 3 had the greatest maximum C_L at Re of 2×10^5, and 3×10^5 while SG6043 modified 1 had the lowest maximum C_L.

Moreover, SG6043 modified 2 had the greatest peak C_L at Re of 4×10^5 to 6×10^5, while SG6043 modified 1 had the lowest peak C_L. Moreover, the SG6043 modified 2 airfoil had the greatest AoA_{stall} at whole Re. At a Re of 10^5 and 2×10^5, the SG6043 modified 2 airfoil had an AoA_{stall} of 12°. Moreover, at Re of 3×10^5 to 6×10^5, SG6043 modified 2 airfoils had an AoA_{stall} of 13°.

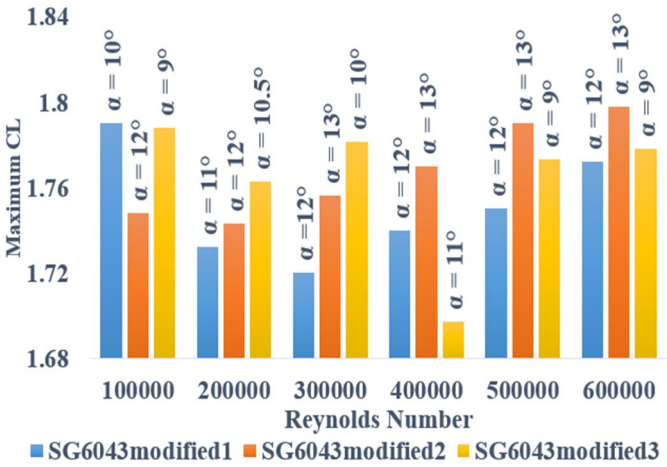

Figure 22. Lift and stall efficiency summary for modified airfoils.

According to **Figure 23**, the SG6043 modified 1 airfoil had the lowest values at a Re of 10^5 to 4×10^5, while the SG6043 modified 2 airfoil had the highest maximum C_L/C_D at a Re of 10^5 and 4×10^5. Moreover, the SG6043 modified 3 airfoil had the highest maximum C_L/C_Dat Re of 2×10^5 and 3×10^5. As well, the SG6043 modified 1 airfoil had the highest maximum C_L/C_D at Re of 5×10^5 and 6×10^5, while the SG6043 modified 3 and SG6043 modified 2 airfoils had the lowest values at Re of 5×10^5 and 6×10^5.

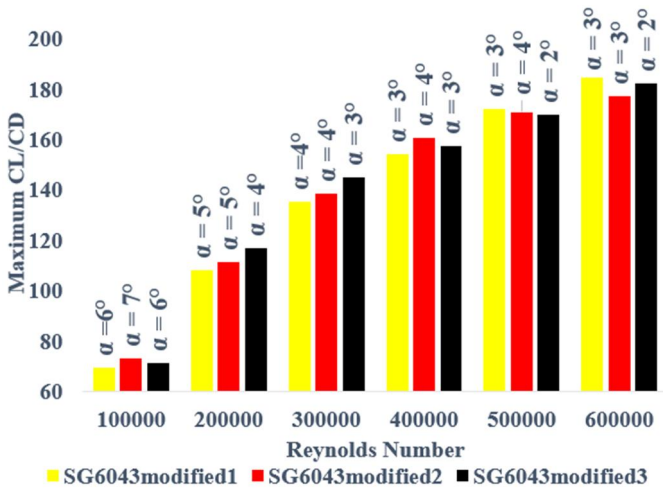

Figure 23. The C_L/C_D efficiency summary for modified airfoils.

The C_L/C_D at Re of 10^5 to 6×10^5 was indicated in **Figures 24–29** and was compared with the findings of other researchers [11,12,29,30] to determine the efficiency of the modified airfoils being compared to other airfoils designed by various studies for low Re and SWT usage.

The C_L/C_D efficiency of the SG6043 modified airfoils and their comparison with another low Re airfoil at Re of 10^5 were presented in **Figure 24**. The SG6043 modified airfoils were compared to the developed airfoils of the EYO-Series [12] at a Re of 10^5. The results revealed that the SG6043 modified airfoils had a higher peak C_L/C_D than the EYO-Series airfoils. Moreover, the SG6043 modified 2 airfoil was more efficient than other airfoils.

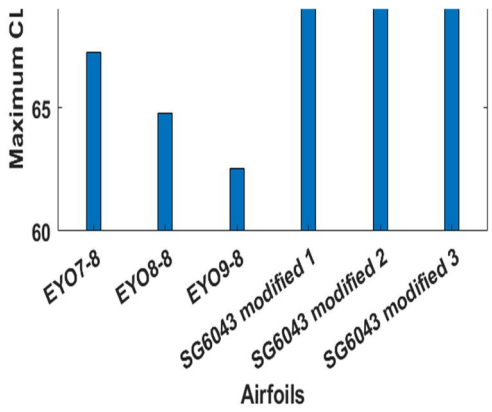

Figure 24. Comparison of SG6043 modified airfoils with EYO-Series airfoils [12] at Re of 10^5.

In **Figure 25**, at a Re of 2 × 10^5, the developed airfoils of the EYO-Series [12] were compared to the SG6043 modified airfoils, and the results demonstrated that the SG6043 modified airfoils had a greater peak C_L/C_D than the EYO-Series airfoils and had a higher efficiency than other airfoils. Additionally, compared to other airfoils, the SG6043 modified 3 airfoil had a higher C_L/C_D.

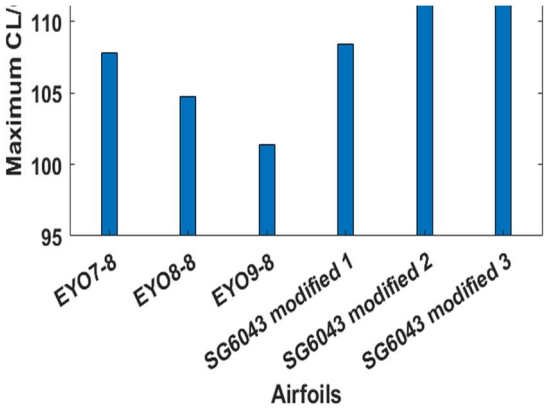

Figure 25. Comparison of SG6043 modified airfoils with EYO-Series airfoils [12] at Re of 2 × 10^5.

Also, at a Re of 3 × 10^5, the SG6043 modified airfoils outperformed the SG604x airfoil family, the EYO-Series airfoils [11,12], and others [9,22] in terms of peak C_L/C_D performance, according to the comparative result in **Figure 26**. Hence, the SG6043 modified 3 airfoils were more efficient than other airfoils.

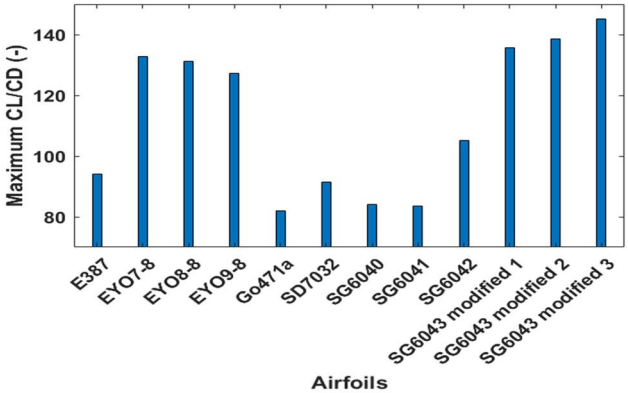

Figure 26. Comparison of SG6043 modified airfoils with EYO-Series [11,12], SG604x airfoil family, and other airfoils [9,22] at Re of 3 × 10^5.

The developed EYO-series [12] airfoils were compared to the SG6043 modified airfoils in **Figure 27** at a Re of 4 × 10^5. The results illustrated that the SG6043 modified airfoils had a higher peak C_L/C_D than the EYO-Series airfoils and higher efficiency than other airfoils. Additionally, compared to other airfoils, the SG6043 modified 2 airfoils were more efficient.

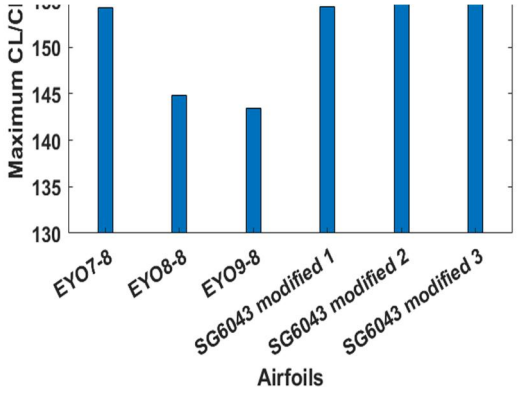

Figure 27. Comparison of SG6043modified airfoils with EYO-Series airfoils [12] at Re of 4×10^5.

The developed EYO-Series [12] airfoils were compared to the SG6043 modified airfoils in **Figure 28** at Re of 5×10^5. The results illustrated that the SG6043 modified airfoils had a higher peak C_L/C_D than the EYO-Series airfoils and higher efficiency than other airfoils. In addition, compared to other airfoils, the SG6043 modified 3 airfoil had a higher C_L/C_D at a Re of 5×10^5.

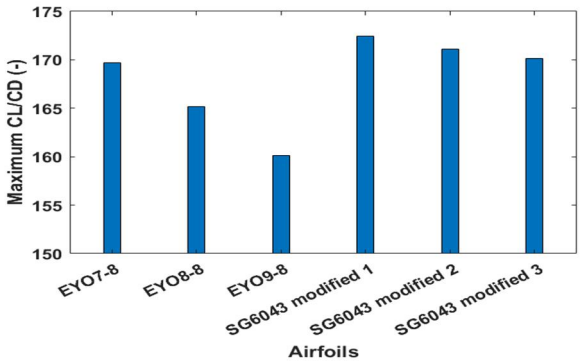

Figure 28. Comparison of SG6043 modified airfoils with EYO-Series airfoils [12] at Re of 5×10^5.

Likewise, compared to other airfoils, the SG6043 modified 3 airfoil had a greater C_L/C_D at a Re of 6×10^5 (**Figure 29**).

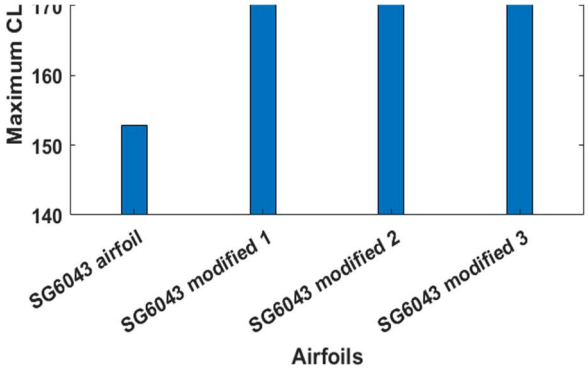

Figure 29. Comparison of SG6043 modified airfoils with SG6043 airfoil at Re of 6×10^5.

5. Conclusions

This study optimized the SG6043 airfoil for low Reynolds number applications by varying the thickness-to-camber ratio (t/c). The results showed that a t/c ratio between 0.5 and 1.5 significantly improved aerodynamic efficiency, with the SG6043 modified 1 airfoil achieving a maximum C_L/C_D of 184.85 at Re = 600,000. The modified airfoils also demonstrated improved stall angles and drag bucket performance, making them suitable for small wind turbines operating at low Re. Future work will include CFD computations, wind tunnel testing, and further optimization of airfoils for different Re ranges. The primary objective of the present research was to find the airfoil with the highest aerodynamic efficiency between 100,000 and 600,000. For the purpose of such a study, 71 effective airfoils from the symmetrical NACA 4-digit, NACA 5-digit, Selig airfoils, Eppler airfoils, and other airfoils were selected for study.

The results showed that the SG6043 airfoil had the greatest maximum C_L/C_D when compared to the other 71 airfoils evaluated at Re from 100,000 to 600,000. To investigate and enhance the form modification of the airfoil utilizing variations in t/c and to determine the ideal t/c at Re of 100,000 to 600,000, the SG6043 airfoil was used. The investigations occurred at Re between 10^5 and 6×10^5, within the usual range for SWT airfoils. According to the research results, efficiency generally improved as the Re increased. The study's major conclusions were as follows.

Based on the findings, 0.5 to 1.5 was the optimum t/c at Re of 100,000 to 600,000 for the development of the SG6043 airfoil, which had the maximum C_L/C_D.

Then, using the XFOIL software, three airfoils were generated with the optimal t/c, and the results revealed that the greatest maximum C_L/C_D values for SG6043 modified 1, SG6043 modified 3, and SG6043 modified 2 were 184.85, 182.36, and 177.25, respectively, at a Re of 6×10^5.

SG6043 modified 2, SG6043 modified 1, and SG6043 modified 3 had peaks C_L of 1.798, 1.79, and 1.788, respectively.

For SG6043 modified airfoils, the AoA_{stall} was from 9° to 13°. For the SG6043 modified 2 airfoil, a maximum AoA_{stall} of 13° was demonstrated for Re of 3×10^5, 4×10^5, 5×10^5, and 6×10^5.

At Re between 3×10^5 and 6×10^5, the airfoils behaved admirably regarding lift efficiency, with no notable changes.

According to the drag bucket analyses, S6043-modified airfoils enhanced lift efficiency to peak lift at either invariable or decreasing drag at all Re.

When compared to the SG6043 airfoil, the maximum C_L/C_D of the SG6043 modified 1, SG6043 modified 2, and SG6043 modified 3 airfoils improved by 5.49%, 10.96%, and 8.32%, respectively, at Re of 100,000.

The maximum C_L/C_D of the SG6043 modified 1, SG6043 modified 2, and SG6043 modified 3 airfoils enhanced in comparison to the SG6043 airfoil by 11.58%, 12.97%, and 20.33%, respectively, at Re of 200,000.

In comparison to the SG6043 airfoil, the maximum C_L/C_D of the SG6043 modified 1, SG6043 modified 2, and SG6043 modified 3 airfoils increased by 15.64%, 18.26%, and 23.68%, respectively, at a Re of 300,000.

The maximum C_L/C_D of the SG6043 modified 1, SG6043 modified 2, and SG6043 modified 3 airfoils enhanced in comparison to the SG6043 airfoil by 16.45%, 21.35%, and 18.83%, respectively, at Re of 400,000.

At a Re of 500,000, the maximum C_L/C_D of the SG6043 modified 1, SG6043 modified 2, and SG6043 modified 3 airfoils rose by 20.30%, 19.36%, and 18.71%, respectively, in comparison to the SG6043 airfoil.

At a Re of 600,000, the maximum C_L/C_D of the SG6043 modified 1, SG6043 modified 2, and SG6043 modified 3 airfoils increased by 20.91%, 16.26%, and 19.28%, respectively, compared to the SG6043 airfoil.

At a Re of 100,000, in comparison to the EYO7-8, EYO8-8, and EYO9-8 airfoils, the SG6043 modified 1 airfoil was able to improve the maximum C_L/C_D by 3.6%, 7.20%, and 11.07%, respectively.

The maximum C_L/C_D of the SG6043 modified 2 airfoil was enhanced by 8.63%, 12.76%, and 16.83% in comparison to the EYO7-8, EYO8-8, and EYO9-8 airfoils, at Re of 100,000.

Compared to the EYO7-8, EYO8-8, and EYO9-8 airfoils, the maximum C_L/C_D of the SG6043 modified 3 airfoil was improved by 6.05%, 12.76%, and 10.07%, respectively, at Re of 100,000.

The maximum C_L/C_D of the SG6043 modified 1 airfoil was increased by 0.64%, 3.59%, and 7.01%, respectively, at a Re of 200,000 when compared to the EYO7-8, EYO8-8, and EYO9-8 airfoils.

Comparing the SG6043 modified 2 airfoil to the EYO7-8, EYO8-8, and EY9-8 airfoils resulted in increases in the maximum C_L/C_D of 3.64%, 6.67%, and 10.20%, respectively, at Re of 200,000.

The maximum C_L/C_D increased by 8.54%, 11.71%, and 15.41%, respectively, at Re of 200,000 when comparing the SG6043 modified 3 airfoil to the EYO7-8, EYO8-8, and EY9-8 airfoils.

When comparing the SG6043 modified 1 airfoil to the EYO7-8, EYO8-8, and EY9-8 airfoils at Re of 300,000, the maximum C_L/C_D rose by 2.20, 3.33, and 6.52%, respectively.

By comparing the SG6043 modified 2 airfoil to the EYO7-8, EYO8-8, and EY9-8 airfoils at Re of 300,000, the maximum C_L/C_D increased by 4.52%, 5.68%, and 8.90%, respectively.

Comparing the SG6043 modified 3 airfoil to the EYO7-8, EYO8-8, and EY9-8 airfoils resulted in increases in the maximum C_L/C_D of 9.30%, 10.52%, and 13.92%, respectively, at Re of 300,000.

When comparing the EYO7-8, EYO8-8, and EY9-8 airfoils to the SG6043 modified 1 airfoil, the maximum C_L/C_D rose by 0.058%, 6.53%, and 7.54%, respectively, at a Re of 400,000.

The maximum C_L/C_D increased by 4.27%, 11.01%, and 12.79%, respectively, at Re of 400,000 when comparing the SG6043 modified 2 airfoil to the EYO7-8, EYO8-8, and EY9-8 airfoils.

At a Re of 400,000, when comparing the EYO7-8, EYO8-8, and EY9-8 airfoils to the SG6043 modified 3 airfoil, the maximum C_L/C_D improved by 2.02%, 8.63%, and 9.66%, respectively.

The maximum C_L/C_D was enhanced by 1.62%, 4.40%, and 7.70%, respectively, at Re of 500,000 when comparing the SG6043 modified 1 airfoil to the EYO7-8, EYO8-8, and EY9-8 airfoils.

The maximum C_L/C_D increased by 0.82%, 3.58%, and 6.85%, respectively, at Re of 500,000 when comparing the SG6043 modified 2 airfoil to the EYO7-8, EYO8-8, and EY9-8 airfoils.

When comparing the SG6043 modified 3 airfoil to the EYO7-8, EYO8-8, and EY9-8 airfoils at Re of 500,000, the maximum C_L/C_D improved by 0.27%, 3.02%, and 6.27%, respectively.

The results revealed that the newly developed EYO-Series airfoils had a lower maximum C_L/C_D than the SG6043 modified 1, SG6043 modified 2, and SG6043 modified 3 airfoils. Additionally, as compared to SG6043 and EYO-Series airfoils, they use fewer materials due to the optimal *t*/*c*, which lowers the cost of production and uses fewer natural resources. Hence, the SG6043 modified airfoils are appropriate for usage in SWT blades due to their aerodynamic performance results.

Furthermore, the modified airfoils at high Re will be compared to the SG6043 airfoil in the upcoming phase of the Solar Turbine Arta Energy (STAE) project. Moreover, a study into other airfoils using *t*/*c* at various Re will be carried out. As a sum up, for the construction of a three-bladed horizontal axis wind turbine, extensive CFD computations, PIV flow visualization, and wind tunnel testing will be carried out.

Author contributions: Conceptualization, HSD and MSD; methodology, MYAJ and MSD; software, MYAJ and MSD; validation, MYAJ, MSD and HSD; formal analysis, MYAJ, MSD and HSD; investigation, MYAJ, MSD and HSD; resources, MYAJ, MSD and HSD; data curation, MYAJ, MSD and HSD; writing—original draft preparation, MSD; writing—review and editing, MYAJ; visualization, MYAJ, MSD and HSD; supervision, MYAJ; project administration, MYAJ; funding acquisition, MSD. All authors have read and agreed to the published version of the manuscript.

Conflict of interest: The authors declare no conflict of interest.

Nomenclature

AoA	The angle of attack (Deg)
AoA_{stall}	stall angle (Deg)
c	chord length (m)
C_L	The lift coefficient (-)
C_D	drag coefficient (-)
D	drag force (N)
l	Airfoil span (m)
L	lift force (N)
L/*D*	lift-to-drag (-)
L/D_{max}	peak lift-to-drag (-)
Re	the Reynolds number (-)
U	Air velocity (m/s)
X/*C*	Relative chord position (-)

Greek letters

ρ	The density of the air (Kg/m^3)
υ	Kinematic viscosity (m^2 s^{-1})
μ	Dynamic viscosity (Kg m^{-1} s^{-1})

References

1. Seifi H, Kouravand S, Davary MS, Mohammadzadeh S. Numerical and Experimental study of the effect of increasing aspect ratio of self-starting force to vertical axis wind turbine. Journal of Renewable and New Energy. 2023; 10(1): 1–14. doi: 10.52547/jrenew.10.1.1
2. Singh RK, Ahmed MR. Blade design and performance testing of a small wind turbine rotor for low wind speed applications, Renewable Energy. 2013; 50: 812–819. doi: 10.1016/j.renene.2012.08.021
3. Akour SN, Al-Heymari M, Ahmed T, Khalil KA. Experimental and theoretical investigation of micro wind turbine for low wind speed regions. Renewable Energy. 2018; 116: 215–223. doi: 10.1016/j.renene.2017.09.076
4. Seifi Davari H, Kouravand S, Seify Davari M, Kamalnejad Z. Numerical investigation and aerodynamic simulation of Darrieus H-rotor wind turbine at low Reynolds numbers. Energy Sources, Part A: Recovery, Utilization, and Environmental Effects. 2023; 45(3): 6813–6833. doi: 10.1080/15567036.2023.2213670
5. Giguere P, Selig MS. Low Reynolds number airfoils for small horizontal axis wind turbines. Wind Engineering. 1997; 367–380.
6. Akram MT, Kim MH. Aerodynamic shape optimization of NREL S809 airfoil for wind turbine blades using Reynolds-averaged navier stokes model—Part II. Applied Sciences. 2021; 11: 2211. doi: 10.3390/app11052211
7. Longtin Martel S, Bashir M, Botez RM, Wong T. A Pareto Multi-Objective Optimization of a Camber Morphing Airfoil using Non-Dominated Sorting Genetic Algorithm. In: Proceedings of the AIAA SCITECH 2023 Forum; 23–27 January 2023; National Harbor, MD, USA. p. 1583.
8. Wu X, Zhang W, Peng X, Wang Z. Benchmark aerodynamic shape optimization with the POD-based CST airfoil parametric method. Aerospace Science and Technology. 2019; 84: 632–640. doi: 10.1016/j.ast.2018.08.005
9. Tirandaz MR, Rezaeiha A. Effect of airfoil shape on power performance of vertical axis wind turbines in dynamic stall: Symmetric Airfoils. Renewable Energy. 2021; 173: 422–441. doi: 10.1016/j.renene.2021.03.142
10. Huang S, Hu Y, Wang Y. Research on aerodynamic performance of a novel dolphin head-shaped bionic airfoil. Energy. 2021; 214: 118179. doi: 10.1016/j.energy.2020.118179
11. Osei EY, Opoku R, Sunnu AK, Adaramola MS. Development of high performance airfoils for application in small wind turbine power generation. Journal of Energy. 2020; 1–9. doi: 10.1155/2020/9710189
12. Osei EY, Opoku R, Sunnu AK, et al. Aerodynamic performance characteristics of EYO-Series low Reynolds number airfoils for small wind turbine applications. Alexandria Engineering Journal. 2022; 61: 12301–12310. doi: 10.1016/j.aej.2022.05.049
13. Hu H, Zhang G, Li D, et al. Shape optimization of airfoil in ground effect based on free-form deformation utilizing sensitivity analysis and surrogate model of artificial neural network. Ocean Engineering. 2022; 257: 111514. doi: 10.1016/j.oceaneng.2022.111514
14. Santos GB, Pantaleão AV, Salviano LO. Using deep generative adversarial network to explore novel airfoil designs for vertical-axis wind turbines. Energy Conversion and Management. 2023; 282: 116849. doi: 10.1016/j.enconman.2023.116849
15. Achour G, Sung WJ, Pinon-Fischer OJ, Mavris DN. Development of a conditional generative adversarial network for airfoil shape optimization. In: Proceedings of the AIAA Scitech 2020 Forum; 6–10 January 2020; Orlando, FL, USA. p. 2261.
16. Lim H, Kim H. Multi-objective airfoil shape optimization using an adaptive hybrid evolutionary algorithm. Aerospace Science and Technology. 2019; 87: 141–153. doi: 10.1016/j.ast.2019.02.016
17. Guo G, Zhu W, Sun Z, et al. Drag reducer design of wind turbine blade under flap-wise fatigue testing. Composite Structures. 2023; 318: 117094. doi: 10.1016/j.compstruct.2023.117094
18. Boudis A, Hamane D, Guerri O, Bayeul-Lainé AC. Airfoil Shape Optimization of a Horizontal Axis Wind Turbine Blade using a Discrete Adjoint Solver. Journal of Applied Fluid Mechanics. 2023; 16(4): 724–738. doi: 10.47176/JAFM.16.04.1493

19. Echavarria C, Hoyos JD, Jimenez JH, et al. Optimal airfoil design through particle swarm optimization fed by CFD and XFOIL. Journal of the Brazilian Society of Mechanical Sciences and Engineering. 2022; 44(11): 561. doi: 10.1007/s40430-022-03866-4
20. Rangriz S, Kheiri M. Design of optimal airfoils for airborne wind energy applications. In: Proceedings of the AIAA SCITECH 2023 Forum; 23–27 January 2023; National Harbor, MD, USA. p. 1155.
21. Kumar S, Narayanan S. Airfoil thickness effects on flow and acoustic characteristics. Alexandria Eng. J. 2022; 61: 4679–4699. doi: 10.1016/j.aej.2021.10.022
22. Song Q, Lubitz WD. Design and testing of a new small wind turbine blade. Journal of Solar Energy Engineering. 2014; 136(3): 4. doi: 10.1115/1.4026464
23. Akuffo FO, Brew-Hammond A, Antonio J, et al. Solar and Wind Energy Resource Assessment (SWERA). Energy Commission Ghana; 2003.
24. Bai CJ, Wang WC, Chen PW, Chong WT. System integration of the horizontal-axis wind turbine: The design of turbine blades with an axial-flux permanent magnet generator. Energies. 2014; 7(11): 7773–7793. doi: 10.3390/en7117773
25. Renganathan SA, Maulik R, Ahuja J. Enhanced data efficiency using deep neural networks and Gaussian processes for aerodynamic design optimization. Aerospace Science and Technology. 2021; 111: 106522. doi: 10.1016/j.ast.2021.106522
26. Acarer S. Peak lift-to-drag ratio enhancement of the DU12W262 airfoil by passive flow control and its impact on horizontal and vertical axis wind turbines. Energy. 2020; 201: 117659. doi: 10.1016/j.energy.2020.117659
27. Wei X, Wang X, Chen S. Research on parameterization and optimization procedure of Low-Reynolds-number airfoils based on genetic algorithm and Bezier curve. Advances in Engineering Software. 2020; 149: 102864. doi: 10.1016/j.advengsoft.2020.102864
28. Singh RK, Ahmed MR, Zullah MA, Lee Y. Design of a low Reynolds number airfoil for small horizontal axis wind turbines. Renewable Energy. 2012; 42: 66–76. doi: 10.1016/j.renene.2011.09.014
29. Giguere P, Selig MS. New airfoils for small horizontal axis wind turbines. J. Sol. Energy Eng. 1998; 120: 108–114. doi: 10.1115/1.2888052
30. Meana-Fernández A, Díaz-Artos L, Fernández Oro JM, Velarde-Suárez S. An optimized airfoil geometry for vertical-axis wind turbine applications. International Journal of Green Energy. 2020; 17: 181–195. doi: 10.1080/15435075.2020.1712211